Crystallization Studies of Highly Monodisperse Oligomeric Poly(Ethylene Oxide)

by

Junjie Yin

A thesis
presented to the University of Waterloo
in fulfillment of the
thesis requirement for the degree of
Master of Science
in
Physics (Nanotechnology)

Waterloo, Ontario, Canada, 2018

I hereby declare that I am the sole author of this thesis. This is a true copy of the thesis, including any required final revisions, as accepted by my examiners.

I understand that my thesis may be made electronically available to the public.

Abstract

Poly(ethylene oxide) is one of the most intensively studied polymers in terms of crystallization, because of its linear structure. In this thesis the chapters are organized in a self-contained fashion, with a general introduction and a brief conclusion. We introduce the purification and characterization of highly monodisperse PEO oligomers, and the analysis of their melting and crystallization behaviours. Through evaporative purification, we have been able to purify low molecular weight PEO, and achieve a polydispersity index six times better than the neat commercial sample, as measured by mass spectroscopy. Melting temperatures are obtained using differential scanning calorimetry. Based on the Gibbs Thomson relation, we claim that during crystallization, some purified PEO samples can form crystal lamellae not only with extended chains, but also with once-folded chains, which is normally not expected for polymers with such short chain lengths. The fact that we are able to control the melting temperature through annealing treatment on the crystal validates our chain-folding model of folded and extended chains.

Acknowledgements

Firstly, I would like to express my sincere gratitude to my supervisor James A. Forrest for his guidance and support in the past two years. He has been an inspirational mentor to me since I first stepped into the world of scientific research. Every discussion with Jamie opens my mind and fuels my motivations to pursue science. Thank you Jamie for being an excellent supervisor.

I would also like to thank my advisory committee members Jean Duhamel and David Hawthorn, who have provided support and helpful suggestions on my research project. I am also grateful to Jean Duhamel and Bae-Yeun Ha, for being on my defence committee, and for their time and effort in reviewing my thesis.

My fellow students and friends in the lab have made my master's study and research a great experience. Adam Raegen, our knowledgeable postdoc in the lab, has been a teacher to me. I have learned useful experimental skills and research methods from him. I would like to thank all former and present members in our lab who have worked with me. Tiana Trumpour, Shipei Zhu, Valentin Ruffine, Neha Dhalwani, Denzil Barkley, thank you for the discussions and talks we have had and the help you provided me. It has been an enjoyable thing to work with these wonderful people.

I am also thankful to Stefan Idziak, who has a long-time collaboration with our lab, and has helped me with experiments in my project. I would like to thank our administrative staff Judy McDonnell, Bonnie Findlay in Physics, and Lisa Pokrajac in WIN for their help. I would also like to thank all the friends I have met in Waterloo. Thank you all for making my life here joyful.

Lastly, I would like to thank my dearest family. Thank my parents Baocai Yin and Ziping Wang for their unconditional love and encouragement throughout my life. Thank my siblings for their kindness. My thanks also goes to my boyfriend Junan Lin, for his love and care, and all the helpful discussions we have had. Thank you all for everything. You mean so much in my life.

Table of Contents

List of Figures

Chapter 1

Introduction

1.1 Polymers

Polymers are large molecules that consist of many repeating units, called monomers. The number of monomers that a polymer contains is defined as its degree of polymerization, N. For a small N value, the polymer is also called an oligomer. Thus the molecular weight of a polymer is $M = NM_{mon}$, where M_{mon} is the molecular weight of a monomer. Typically, the backbone of a polymer is composed of carbon atoms connected to each other by covalent bonds. Polymers that contain only one type of monomer are called homopolymers, while those containing more than one type are called heteropolymers, or copolymers [1].

Polymer samples normally exist as a collection of polymer molecules with usually unequal molecular weights, hence the molecular weight distribution of the entire sample can be described using both number average molecular weight, M_n, and weight average molecular weight, M_w:

$$M_n = \frac{\sum N_i M_i}{\sum N_i} \tag{1.1}$$

$$M_w = \frac{\sum N_i M_i^2}{\sum N_i M_i} \tag{1.2}$$

where M_i is the molecular weight of a polymer chain, and N_i is the number of polymer chains with molecular weight M_i. On both sides of M_n, there are equal numbers of polymers, while on both sides of M_w, there are equal weights of polymers.

Polydispersity index (PDI) is defined by the ratio of M_w to M_n, and it describes how broad the molecular weight distribution is. If all the polymers in a sample have the same degree of polymerization, PDI is equal to 1, and the sample is called monodisperse. The larger PDI is, the broader the molecular weight distribution is. In studies on properties that are sensitive to the value of N, a small PDI is normally preferred because it is easier to look at individual N's. For an intuitive sense of PDI, here is an example. A sample contains half, by number, of polymers with molecular weight 1000, and the other half with molecular weight 2000. M_n of this sample is calculated to be 1500, and M_w is 1667. Thus PDI of this sample is 1.11, which appears decent, but the corresponding sample is far from pure. In real cases the polymers are more likely to have a smoother distribution of different molecular weights rather than shown in this particular example, but this calculation gives us an idea of how PDI could be hiding the actual composition of a polymer sample, and shows that M_w and M_n are not enough to fully describe the distribution.

1.2 Polymerization

Synthesized polymers contain a distribution of different molecular weights. Even the most monodisperse synthetic polymers have a polydispersity index (PDI) of about 1.01 [2], which still contain many different N values. This fact is closely related to the process of producing synthetic polymers, polymerization.

Polymerization is the process of connecting monomers together onto a polymer chain. This process can be achieved through different methods. Common methods include step-growth polymerization, chain-growth polymerization, and living anionic polymerization,

which is a special case of chain-growth.

Step-growth polymerization refers to the process in which stepwise reactions among functional groups of monomers form polymers. Typical polymers produced by step-growth include polyamide (nylon), polyester, and polyether [3]. Chain-growth polymerization refers to the process in which monomers are added onto the active sites of a growing polymer successively. Typical polymers produced by chain-growth include polyethylene, polypropylene, and polyvinyl chloride [4]. Being a special case of chain-growth, living polymerization is a process in which the termination step of the polymer growth is eliminated, and the rate of chain initiation is much larger than chain propagation, making the polymer growth easier to control.

As they are based on different mechanisms, these methods lead to different polydispersity indices. The typical PDI that step-growth leads to is around 2, and for common chain-growth such as free radical polymerization, it is $1.5 \sim 2$. Living anionic polymerization normally leads to a PDI less than 1.2, which can even reach a number very close to 1, provided proper conditions [5].

1.3 Poly(ethylene oxide)

Poly(ethylene oxide), also known as poly(ethylene glycol) or poly(oxyethylene), is a polymer with the repeating unit:

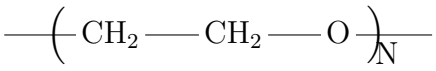

PEO can be found in macromolecules having various architectures, including linear, branched, star and comb, and the most widely used type in industry, especially for high molecular weights, is linear PEO. It is soluble in water, acetone, benzene, dichloromethane, chloroform, ethanol, methanol, etc., depending on its molecular weight [6].

Low molecular weight PEO (normally below 400 g/mol) is liquid at room temperature, and its melting point increases with increasing molecular weight, with an upper limit of

68.9 °C [7], which is the predicted melting temperature of PEO in the limit of infinite molecular weight.

PEO based materials have advantages over other materials such as non-toxicity, low cost, and electrochemical stability [8]. Therefore they have a wide range of applications in fields including biology, chemistry, and medicine. Because of its excellent ion conductivity, one of the most promising applications is to act as electrolyte material in lithium ion batteries [9]. However, it is the amorphous phase in PEO that contributes to ion conductivity, while the linear structure of PEO leads to high crystallinity, which restrains ion transportation especially at low temperatures. Thus, further research on PEO crystallization is of great importance.

In this research, the PEO sample purchased from Sigma Aldrich, Inc. has an M_n of 600 g/mol, which appears as waxy solid at room temperature. Both ends contain hydroxy groups only. The polydispersity index is not specified in the product information.

1.4 Importance of N

The degree of polymerization N has an important effect on many properties of polymers. For instance, in calculations of solubility and mixing of solutions as in the Flory-Huggins equation [1]:

$$\Delta F_{mix} = kT[\frac{\phi}{N}\ln\phi + (1-\phi)\ln(1-\phi) + \chi\phi(1-\phi)] \tag{1.3}$$

where ΔF_{mix} is the free energy of mixing a polymer with a solvent, k is Boltzmann's constant, T is temperature, ϕ is the volume fraction of the polymer, N is the degree of polymerization, and χ is the Flory interaction parameter (dimensionless). This equation shows that different N's cause different solubilities.

Another property that N influences is glass transition temperature T_g. Glass transition is one of the most crucial phase transitions in polymer science, which refers to the tem-

perature at which the free volume available for molecular motions achieves a minimum. According to Fox-Flory equation [10]:

$$T_g = T_{g,\infty} - \frac{K}{M_n} \tag{1.4}$$

where $T_{g,\infty}$ is the maximum glass transition temperature that can be achieved at a theoretical infinite molecular weight and K is an empirical parameter that is related to the free volume present in the polymer sample. T_g is dependent on M_n, which is directly determined by N.

Polymer crystallization is also affected by N. One example is atactic polystyrene (aPS). Atactic indicates that the phenyl groups are randomly oriented along the chain. Therefore, crystallization is less preferred for aPS, and thus it has been described as a non-crystal. However, using atomic force microscope (AFM), Yu Chai *et al* [11] observed crystal formation in aPS samples with $M_w = 600g/mol$, which corresponds to a very low N. This indicates that N has significant effects on polymer crystallization.

One of the many effects of N values on polymer crystallization is related to the end groups. End groups normally contribute to amorphous regions in polymer crystals, and they influence crystal formation process. With different N values, the fractions of end groups are different, which changes the extent of their effect. Therefore, to fully explore the effect of N, polymer fractions with different N values must be isolated first.

1.5 Polymer crystallization

Crystallization of large molecules has long been a research topic intensively studied, yet with numerous questions unsolved and mechanisms to be understood. The main factor that causes the essential difference in polymer crystallization and crystallization of a regular small molecule is the long chain nature of a polymer, which results in very different kinetic mechanisms than small molecules. Long chains could easily get entangled, which prevent themselves from being aligned in order in the crystalline lattice. However, crystallization

is still possible in certain polymers, often with a much different structure than regular crystals.

In this thesis, PEO is our subject of crystallization study. This linear polymer has many properties in common with n-alkanes, therefore studies on n-alkane crystallization could also give us insights into our research. For n-alkane crystallization from melt, investigations have been focused on aspects including crystal structure, chain conformations, nucleation and growth mechanisms. Conformation of n-alkane chains in the crystal include both extended chains and folding of chains [12, 13], where the number of folds depends on chain length and crystallization conditions such as temperature. Nucleation and growth rates of n-alkane crystals have also been investigated, and most studies are based on experimental methods including X-ray diffraction (XRD), small angle X-ray spectroscopy (SAXS), infrared spectroscopy, optical microscopy, and electron microscopy, as well as computer simulation methods such as molecular dynamics (MD) simulations [14, 15].

In Chapter 3, a more detailed review on polymer crystallization and PEO crystallization in particular is provided, mainly focusing on the thermodynamics and crystal structure. In Chapter 4, polymer crystallization kinetics, including nucleation and crystal growth mechanisms are reviewed.

Chapter 2

Evaporative purification

In order to study the effects of N, the first thing needed is to obtain very monodisperse samples with different N values. This has been achieved through an evaporative purification technique, which has been practised on low molecular weight polystyrene, and proved to be an efficient way to obtain highly monodisperse polymers [16].

2.1 Vapour pressure of PEO oligomers

For a particular polymer, as its N decreases, its vapour pressure increases, and for polymers with small enough N values, their vapour pressure could be significant at high temperatures (lower than their thermal degradation temperature). This fact potentially allows one to separate polymer components with different N values, by applying an evaporation method similar to distillation.

To examine the feasibility of separating components through evaporation, it is a good idea to first look at their vapour pressures. Unfortunately, there are few data of vapour pressure of pure PEO [17], either from calculation or experimental measurements. Therefore, we applied a theoretical model to calculate the vapour pressures of low molecular weight PEO.

Sanchez and Lacombe's Lattice-Fluid Model [18] describes a fluid using only three molecular parameters, and provides a method to calculate the relation between vapour pressure and temperature for a given N value. These three parameters for PEO could be found in the literature [19].

In this model, Gibbs free energy G is a function of mass density ρ:

$$G = -\rho + P\nu + T[(\nu - 1)\ln(1 - \rho) + \frac{1}{r}\ln(\rho/\omega)] \tag{2.1}$$

where ρ is reduced density, P is reduced pressure, ν is reduced volume, T is reduced temperature, r is the number of monomers in a polymer molecule, and $\omega = \delta r/\sigma e^{r-1}$ (δ is the flexible parameter, and σ is the symmetry number). For a specific N at given pressure and temperature, G could be plotted as a function of ρ as shown below.

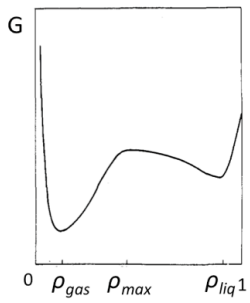

Figure 2.1: Gibbs free energy vs mass density, where a liquid phase is metastable with respect to the vapour phase. Figure source: "An elementary molecular theory of classical fluids. Pure fluids" by Isaac C. Sanchez *et al*, *J. Phys. Chem.*, 80(21):2352-2362, 1976 [18].

The curve has two local minima. The first minimum represents the gas phase, with lower mass density, and the second minimum represents the liquid phase, with higher mass density. By tuning pressure or temperature, the two minima can be adjusted to be equal. This means the system has equal probability to be in the state of either gas or liquid. At a given temperature, there exists only one pressure that satisfies this equality, and this pressure and temperature are defined as the saturation pressure and temperature. The locus of all the saturation points represents the saturation/coexistence line, which is in

fact the curve of vapour pressure as a function of temperature.

Solving Equation 2.1 and applying the three molecular parameters found in literature, we were able to calculate the vapour pressure curve for each N value of PEO oligomers. The results are shown in the plot below, and note that each curve has been generated from 10-20 calculated points.

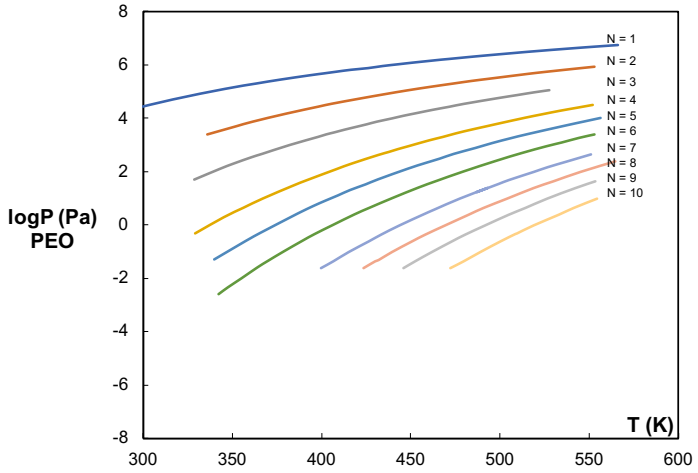

Figure 2.2: Plot of vapour pressure vs temperature for PEO oligomers with N values from 1 to 10.

The results for vapour pressures calculated from this model are not expected to be numerically correct, but they provides a good guidance in terms of the trend of vapour pressure curves and the gaps between neighbouring N's. For a specific N, vapour pressure increases with temperature; for a specific temperature, vapour pressure decreases with N. More importantly, at a given temperature, the vapour pressures of two neighbouring N's have a difference of up to two orders of magnitude. However, this difference gets smaller as temperature goes higher, which indicates that it would be increasingly difficult to achieve a perfect separation, and the purification products are expected to be more polydisperse under higher evaporation temperature. In addition, the comparison between vapour pressures of PS [16] and PEO implies that it is harder to separate individual N's of PEO, because the spacings among curves are narrower for PEO than for PS, and thus

the evaporation products of PEO might not be as good as PS. Evaporation temperature should never get close to 533K [20], which is the critical temperature where PEO begins thermal degradation in vacuum.

2.2 Evaporation technique and results

The experimental setup for evaporative purification is generally the same as the setup used for polystyrene [16]. 96 mg of neat PEO 600 g/mol sample is placed on top of a polished silicon wafer of 2 cm $\times$ 2 cm in size and 0.3 mm in thickness. The Si wafer acts as a bottom substrate and is placed onto a Linkam hot stage in a home-built vacuum chamber. In order to collect depositing fractions, another Si wafer of 5 cm $\times$ 5 cm in size is held approximately 3 mm directly above the neat material, by thermal insulating spacers.

Before the beginning of each evaporation period, the chamber is pumped down with a dry scroll pump to an initial pressure of around 0.3 mbar. After that, we flush the chamber with nitrogen, and then evacuate it again. This process is repeated several times to flush out oxygen in the chamber, so to prevent oxidation of the polymer. Three times of flushing leads to an oxygen level of approximately 4.7×10^{-6} times the oxygen level in atomsphere. Finally, we introduce a small amount of nitrogen into the chamber, until the pressure is raised to about 170 mbar. The reason for this action is because during the evaporation, the system requires a good thermal conduction to drive away excess heat from the hot stage, so to maintain a stable temperature (with a fluctuation of less than 1K) of the material.

We start the evaporation from 393K, and the evaporated material is collected every two hours. Products from the first four hours are not collected, as they may contain impurities such as initiators. We seal the product from each period into an aluminum sample pan, in preparation for future differential scanning calorimetry measurements and mass spectroscopy measurements.

Figure 2.3 shows that within each temperature region during the evaporation, the mass of material collected experiences a general decreasing trend. The mass of products collected into sample pans from the top substrates ranges from 0.2 mg to 2.9 mg. We expected that

small N's would come off first, and as we increased the temperature, higher N's would come off later. Therefore, the neat sample would get purified through separating different N's.

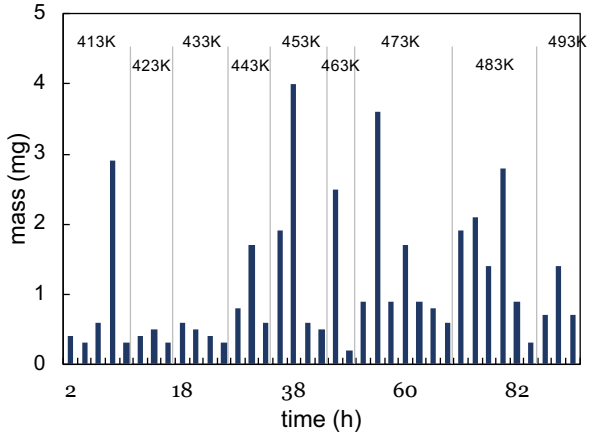

Figure 2.3: Mass of PEO deposited on top substrate with respect to time and temperature.

2.3 Results from mass spectroscopy

To obtain information about the actual distribution of different N's in each fraction, mass spectroscopy measurements were performed on several samples. Matrix Assisted Laser Desorption/Ionization – time of flight (MALDI-TOF) technique was applied, with a Bruker Autoflex Speed MALDI-TOF mass spectrometer to conduct the measurements.

A typical MALDI-TOF mass spectroscopy measurement works with the following procedure:

- Mix the analyte (polymer sample in our case) with appropriate matrix material (dithranol in our case).
- Bombard the mixed material with laser. The laser energy is absorbed by the matrix, which get desorbed and ionized, and a phase transition from solid to gas takes place in the matrix material.

- A hot plume is generated, and during the flight of both the matrix material and the analyte, collisions among particles could result in the ionization of the analyte.
- Ions flying into the the TOF mass spectrometer are separated due to different mass (m)-to-charge (z) ratios. With the same kinetic energy, lighter ions arrive at the detector earlier than heavier ions, according to the equation:

$$\frac{m}{z} = \frac{2eUt^2}{L^2} \tag{2.2}$$

  where e is the electron charge, U is the voltage applied to create the electric field, t is the time of flight, and L is the path length.

From the spectrum generated, the exact distribution of molecular weights can be obtained, from which M_n, M_w, and PDI can be calculated.

2.3.1 MALDI-TOF spectra and analysis

MALDI measurements were carried out for 10 samples out of all the fractions, the neat PEO sample, and the leftover sample after all the evaporation periods. Figure 2.4 is the spectrum of the neat sample, with M_n and M_w indicated by arrows on the plot. Figure 2.5 compares the purified fractions and shows the changes in molecular weight distribution during the evaporation process, with the green background spectrum being the neat sample.

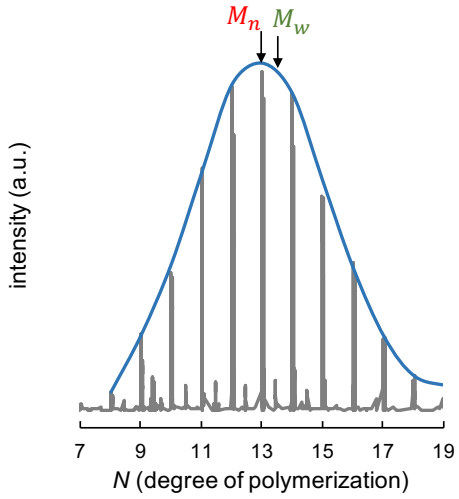

Figure 2.4: MALDI spectra of the neat sample, with M_n and M_w indicated.

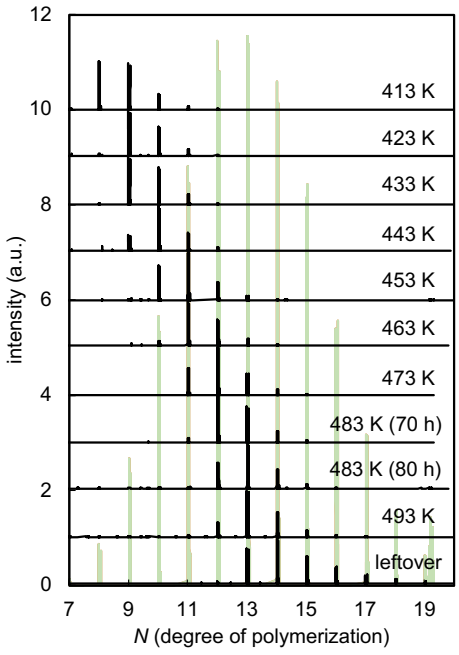

Figure 2.5: MALDI spectra of purified products (black) and neat sample (green) (80 h: 80th hour since start of evaporation).

As the evaporation temperature increases, the N values of the PEO chains composing each fraction shift towards higher values, ranging from 8 to 16. With the intensity of each peak, we are able to calculate their M_n, M_w, and PDI, and make quantitative comparisons. Compared to the neat sample, the N composition of the products are much narrower, meaning they are highly monodisperse. The lowest PDI of the products is calculated to be 1.0052, and $(PDI - 1)$ is around six times better compared to 1.0306 of the neat sample.

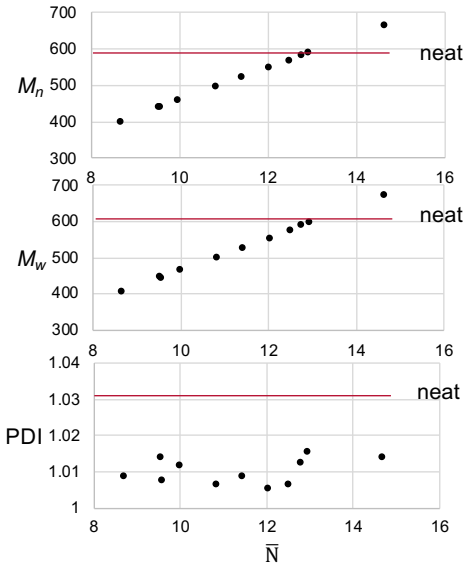

Figure 2.6: M_n, M_w, and PDI comparison between products and neat sample.

2.3.2 Evolution of N during evaporation process

So far the distribution of N's at these 10 points during evaporation is obtained. However, it would be ideal if we could generate the evolution of N values at any point without doing MALDI measurements on every single sample. In order to achieve this, we first plot the evolution of each N value as a function of evaporation time, based on the number fraction of each N in the products from different points during the evaporation process. Then we fit the ten data points for each N value with Gaussian curves, which enables us to estimate the distribution of all N's at any point during the evaporation (by applying interpolation

only) (Figure 2.7), and therefore calculate estimates of M_n, M_w, PDI of samples that did not have MALDI performed.

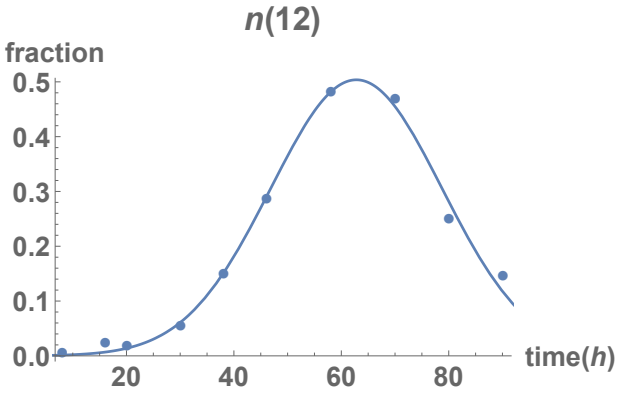

(a) Number fraction of $N = 12$ in samples from different evaporation time.

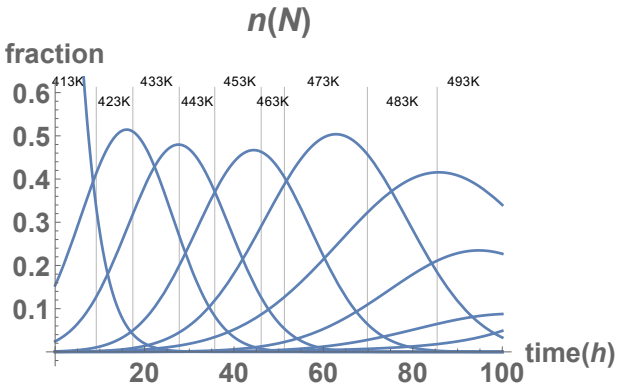

(b) Evolution of N values (from 8 to 16).

Figure 2.7: Evolution of N values during evaporation process.

Chapter 3

Chain conformation analysis

3.1 Polymer crystallization

3.1.1 Polymer crystal models and theories

Material systems naturally tend to stay in a lower energy state. Therefore a regular liquid composed of small molecules, upon cooling, will transition into the solid state (the ground state), becoming either amorphous or crystalline. The true ground state for a polymer corresponds to the situation of all monomers extended and aligned parallel with each other. However, since the chains are relatively long and randomly aligned in the liquid state, it is much more difficult for the polymer to achieve this ground state. Instead, polymers can still crystallize under proper conditions, adopting more complex structures rather than the ideal crystalline state. This process does not only depend on thermodynamics, but kinetics as well.

Before examining long polymers chains, oligomers (especially linear ones) are a simpler yet close enough example in terms of crystallization. Based on X-ray crystallography results, oligomer crystals adopt a structure of stacked layers, with each layer composed of chains standing up perpendicular to the layer surface (Figure 3.1) [21]. Among neighbouring layers, end-groups of the chains form an amorphous phase at the interfaces (not shown

in the drawing).

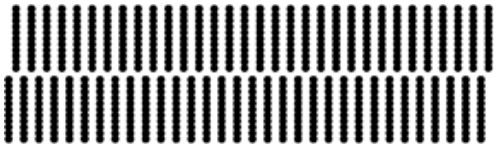

Figure 3.1: Oligomer crystal structure. Figure source: "The physics of polymers: Concepts for understanding their structures and behaviour" by Gert Strobl, 2007 [21].

For crystallization of polymers with higher molecular weights, however, it is impossible for the chains to completely disentangle, which would require an extremely high energy and a very long time. Limited by the nature of polymers themselves, the chains align into local crystalline domains, with some unresolved entanglements left as amorphous phases in between. Similar to oligomers, end-groups are also part of the amorphous phase. Therefore, polymer crystals are called semicrystalline crystals.

Fringed micelle model

In order to describe semicrystalline polymer crystal structures in further details, different models and theories have been proposed. One of the earliest (in 1930) models is the fringed micelle model [22], as shown in Figure 3.2. In this model, both the crystalline phase and the amorphous phase are present, with the crystallites existing as local domains. The micelles of crystalline parts have sizes much smaller than the chain lengths, so a single polymer chain is believed to be able to pass through several micelles, thus binding them together.

Figure 3.2: Fringed micelle model of polymer crystal structure. Figure source: "Principles of polymer chemistry" by Paul J. Flory, *Cornell University Press*, 1953 [23].

However, there were some problems with the fringed micelle model. According to the calculation of free energy, it was found that there would be a large conformational entropy loss for the amorphous chains if this model was true [24]. In addition, experimentalists observed evidences of large crystallites - "spherulites", which have a strong preference in terms of the alignment of chains, and are highly symmetrical instead of a random distribution of crystallites [25]. Together with some other flaws and contradictions found with the model itself [26, 27], people began to doubt the fringed micelle model and tried to find other ways to describe semicrystalline polymer crystals.

Folded chain model

As the fringed micelle model was being questioned, some crucial experimental observations led to the birth of a new model of polymer crystals—the folded chain model. The concept of chain-folding was first proposed by Storks [28]. He observed unstretched films of gutta-percha through electron diffraction measurements, and found that the films were composed of large crystallites with the chain axis perpendicular to the film surfaces. The thickness of the films were much smaller than the chain lengths, which led to Storks' proposal that the chains need to fold themselves inside the film. At that time (1938), the fringed micelle model was dominating the directions of polymer crystallization research, so his results and proposal did not receive much attention. Later, several researchers [29, 30, 31] studied polymer single crystals and found that they have smooth surfaces, with heights of about 10

nm, which was also much smaller than the chain lengths used in those studies. The chains are believed to fold themselves back and forth in the layer, and when the polymer solution concentration is high enough, or when the polymer crystallizes from a melt, multiple layers stack together to form a crystal, with each layer called a lamella. These observations helped the development of the folded chain model, which from then on became the most widely accepted model of polymer crystals.

Now it is clear that the chains fold in crystals. The next step is to determine the way the chains fold. After the chain gets to the amorphous interface and folds back on itself, it is not clear where it re-enters the lamella. There have been a large number of studies on this [32, 33, 34] and two major models have been proposed: adjacent re-entry and random re-entry.

As the adjacent re-entry model describes, after a chain escapes the lamella and makes a fold, it turns right back and inserts into the neighboring site. In this way, the lamellae created have relatively smooth surfaces, as Figure 3.3 shows.

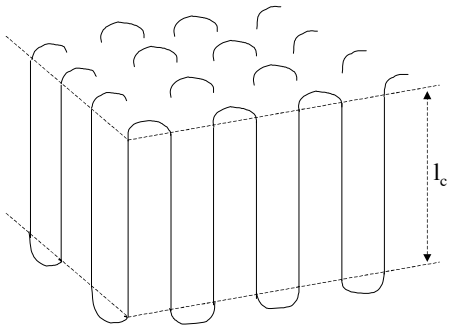

Figure 3.3: Adjacent re-entry model of polymer crystals. Figure source: "On the Morphology of the Crystalline State in Polymers" by P. J. Flory, *J. Am. Chem. Soc.*, 1962 [24].

The random re-entry model is also known as the switchboard model. Instead of folding right back into the neighbouring site on the same lamella as in the adjacent re-entry, a chain that emanated from the lamellar surface could either float on the interface and walk into a further site, or even bridge across to another lamella crystal (not shown in Figure

3.4), which leads to a completely random arrangement on the interfaces of lamellae and amorphous regions (Figure 3.4).

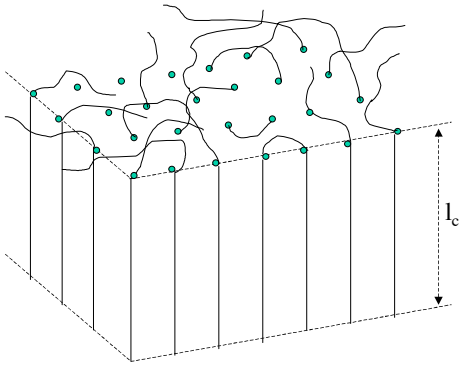

Figure 3.4: Random re-entry model of polymer crystals. Figure source: "On the Morphology of the Crystalline State in Polymers" by P. J. Flory, *J. Am. Chem. Soc.*, 1962 [24].

The adjacent re-entry model would result in a much more thermodynamically favourable conformation with a lower entropy. However, in a real situation of polymer crystallization, twisting, misalignment, and entanglements of the long chains prevent them from relaxing and aligning perfectly in regular folds within the time available. Instead, regions consisting of too many entanglements are more likely to be shifted to the surfaces and contribute to the amorphous phase [21]. Taking both thermodynamics and kinetics factors into account, real polymer crystal lamellae are normally composed of both adjacent re-entries and random re-entries. It should be noted that in real cases, chain-folding also depends on more factors (e.g. chain lengths, flexibility of chains, crystallization temperature, cooling rate, chain defects).

3.1.2 Thermodynamics of polymer crystallization

In terms of thermodynamics, the most favourable state for polymers is the state with the lowest possible Gibbs free energy G. G is lower for a melt than for crystals at high temperatures, while it is lower for crystals than for melt at low temperatures. The equilibrium

melting point T_m^∞ is defined as the temperature at which the liquid state and the solid state have the same free energy. Therefore, the change in the Gibbs free energy, ΔG, is equal to zero during melting or crystallization at thermodynamic equilibrium:

$$\Delta G = \Delta H - T_m^\infty \Delta S = 0 \tag{3.1}$$

$$T_m^\infty = \frac{\Delta H}{\Delta S} \tag{3.2}$$

In practical cases, the crystallization temperature T_c is always lower than the melting temperature T_m, and their difference is defined as the supercooling ΔT. This is mainly due to the nucleation and growth mechanism during crystallization. A nucleus must be present to initialize the growth of a crystal, and when there is no present nuclei, the temperature is able to keep decreasing until the melt itself starts a primary nucleation. This mechanism will also be further discussed in Chapter 4. ΔT of polymers can be as large as 20 to 30 K, resulting from the metastable chain-folding nature of polymers [35].

Equation 3.2 tells us that the equilibrium melting temperature depends on both the enthalpy and the entropy of the system. However, the effect of surface energy and crystal size has not been considered. For a real polymer crystal, the shape and size of the lamella will directly affect its melting point, and this effect can be examined through thermodynamics.

Let us start with an infinitely large, perfect crystal, that from a conventional thermodynamic viewpoint is considered not to involve surface energy. Therefore its melting point is to be T_m^∞.

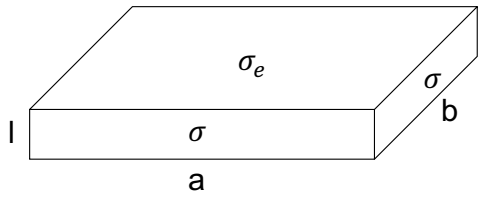

Figure 3.5: Schematic drawing of a polymer crystal lamella.

Now assume a lamella (Figure 3.5) with length a, width b, and height l, where $a \gg l$, and $b \gg l$. The surface energy per unit area of the top and bottom surfaces is σ_e, and the surface energy per unit area of the side surfaces is σ. This lamella with the finite size effect could be considered as a quasi-two dimensional object with one-dimensional confinement [36]. The free energy per unit mass on melting is Δg, and the total free energy ΔG on melting consists of the energy required to create new surfaces and the energy of fusion for the bulk:

$$\Delta G = 2(a+b)l\sigma + 2ab\sigma_e - abl\Delta g \tag{3.3}$$

and with $\sigma_e \gg \sigma$, $a \gg l$, $b \gg l$, the total free energy is then:

$$\Delta G = 2ab\sigma_e - abl\Delta g \tag{3.4}$$

At the melting temperature T_m, $\Delta G = 0$, which leads to:

$$\Delta g(T_m) = \frac{2\sigma_e}{l} \tag{3.5}$$

Once again, for an infinitely large crystal, we have:

$$\Delta g(T_m^\infty) = \Delta h(T_m^\infty) - T_m^\infty \Delta s(T_m^\infty) = 0 \tag{3.6}$$

Assuming between T_m and T_m^∞, the enthalpy and entropy could be treated as invariant, we further have:

$$\Delta g(T_m) = \Delta h(T_m) - T_m \Delta s(T_m) \tag{3.7}$$

Combining Equation 3.6 and Equation 3.7, we are able to generate:

$$\Delta g(T_m) = \Delta h(T_m) - T_m \frac{\Delta h(T_m)}{T_m^\infty} \tag{3.8}$$

Now with Equation 3.5 and Equation 3.8, we finally obtain the relation between the thickness of a lamella and its melting temperature:

$$T_m = T_m^{\infty}(1 - \frac{2\sigma_e}{l\Delta h}) \tag{3.9}$$

which is the well-known Gibbs Thomson equation. It has been applied to many polymers with linear structure and has proved to provide reliable predictions of the melting temperature as a function of lamella thickness [37]. With a larger thickness, the finite size effect is weaker, and the melting temperature T_m of the lamella is closer to the equilibrium melting temperature T_m^{∞}.

3.2 PEO crystallization

In terms of crystallization, PEO is one of the most intensively studied polymers, together with polyethylene and the n-alkanes. With linear structures, these polymers all crystallize very easily. As a semicrystalline polymer, PEO chains fold into lamellar structures during crystallization, and multiple lamellae stack up to form the whole crystal [38]. In our case, we focus on low molecular weight PEO, so crystallization should be even easier since the chains are relatively short and thus need to fold fewer times. When the number of folds changes, the thickness of the lamella varies, which has a direct influence on the melting temperature of the crystal lamella, as discussed in the previous section.

3.2.1 Crystal structure

PEO crystals have monoclinic unit cells, with the chains adopting a structure of 7/2 helix with trans-gauche-trans conformation. In this conformation, seven monomeric units form two periods of the helix, which is 1.93 nm long [39]. As shown in Figure 3.6, every bond is rotated by a certain angle with respect to the c-axis (vertical axis) of the lamella, and the projection length of one monomer on the c-axis, l_c (or h as in the figure), is 0.278 nm [40].

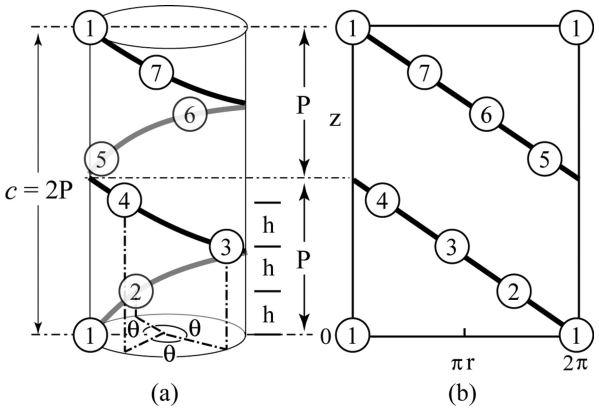

Figure 3.6: 7/2 helix structure (a) and its radial projection (b). Circles with numbers represent monomers. Pitch length, P, and unit length, h, represent the axial lengths of one helical turn and one monomer, respectively. θ represents the angle between two monomers around the helical axis, and r represents the helix radius. Figure source: "Revisiting the Molecular Structure of Collagen" by Kenji Okuyama, *Connect. Tissue Res.*, 49(5):299-310, 2008 [41].

Low molecular weight PEO fractions, or PEO oligomers, crystallize with chains folded a small number of times, or even fully extended [32, 42]. The number of folds depends on many factors including crystallization temperature, chain length, and cooling rate. The thickness of the lamella L is thus determined by the number of folds n and the chain length λ:

$$L = \frac{\lambda}{1+n} = \frac{Nl_c}{1+n} \tag{3.10}$$

where N is the number of monomers in a chain, or the degree of polymerization. In the special case of fully extended chains, $n = 0$, and the thickness of the lamella is equal to the chain length. The lower molecular weight limit for a PEO chain to adopt the folded configuration is reported to be 2000 g/mol, which correspond to 45 monomers [32]. Chains shorter than this have been believed to have the extended configuration only.

In terms of chain folding, we have also discussed the two different chain re-entry models in 3.1.1: adjacent re-entry and random re-entry. In the case of PEO oligomers, the chains

are relatively short, so they are easier to get aligned, and we could expect more adjacent re-entries in the lamellae. On each chain fold on the lamellar surfaces of low molecular weight PEO, it costs 3.5 monomers on average to complete a 180-degree turn, which correspond to half of the 7/2 helix [43].

3.2.2 Melting points of PEO oligomers

The Gibbs Thomson equation (Equation 3.9), enables one to build the relation between melting points and other physical parameters of a polymer crystal. In order to be consistent with other research on PEO melting transitions, here we make some modifications to the original equation:

$$T_m = T_m^{\infty}(1 - \frac{2SV}{L\Delta H}) \tag{3.11}$$

where S is the surface free energy of the interface between the crystalline and the amorphous phase, and V is the molar volume of a crystallizable repeat unit [44]. In this equation, T_m^{∞}, V, and ΔH are constants that have been determined for PEO.

Melting transitions of PEO have been intensively studied through various experimental methods and from different theoretical aspects. One of the fundamental studies is of particular interest to us and is worth being reviewed. Monodisperse PEO oligomers with a degree of polymerization ranging from 9 to 45 were produced through step-wise syntheses by Yeates *et al* [45]. Melting points of these fractions were measured, and compared to those of commercially available samples, which were much more polydisperse. Their results are shown in Figure 3.7.

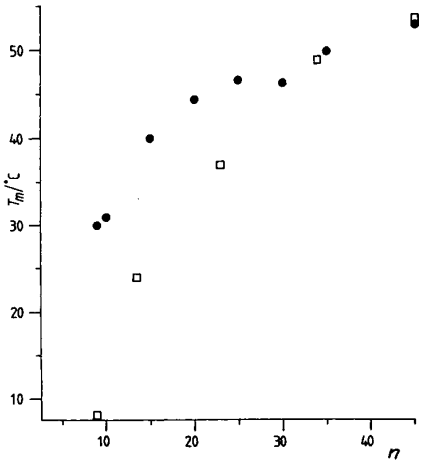

Figure 3.7: Melting points vs degree of polymerization for monodisperse (black dots) and polydisperse (empty boxes) PEO oligomer samples (n was used here in place of N). Figure source: "Ethylene glycol oligomers" by Stephen G. Yeates *et al*, *Makromol. Chemie*, 185(8):1559-1563, aug 1984 [45].

Melting points of monodisperse samples are notably higher than those of polydisperse samples in general, and the difference is especially large for small N values. This observation indicates that polydispersity has a big influence on melting temperature, and in fact motivated us to conduct crystallization experiments with our purified samples, so that we could further investigate this phenomenon.

As a matter of fact, this observation has attracted much attention from researchers. One of the explanations that has been proposed suggests that the T_m difference could be related to the chain end-groups [46]. In a relatively monodisperse sample, chains have roughly the same length, which makes it easier to create a smooth lamellar surface, and the end-groups would be incorporated in the crystalline array. However, in a polydisperse sample, the distribution of chains results in a more disordered lamellar surface, so some of the end-groups have to be incorporated in the amorphous phase. Because of the difference in the incorporation of chains ends, polydisperse crystals would have lower crystallinity and higher entropy, which leads to a higher melting temperature.

3.3 Basics of differential scanning calorimetry

3.3.1 Phase transitions in polymers

Phase transitions are important to characterize the properties of a given polymer. In regular materials, phase transitions normally refer to the transitions between solid, liquid, and gaseous states. For polymer materials, we focus more on the transition between solid and liquid, i.e., melting transition and crystallization transition, which occur in the crystalline regions in polymers. In addition, there is a unique transition that takes place in the amorphous regions of polymers – namely the glass transition.

In crystalline regions, materials stay in the form of disordered melt at temperatures above T_m, and ordered crystalline solid below T_m. As shown in Figure 3.8, at the melting temperature T_m, the material experiences a discontinuity in the specific volume, and absorbs or releases a certain amount of heat (depending on the direction of transition), which is called latent heat. Such transitions are classified as first-order phase transitions [47].

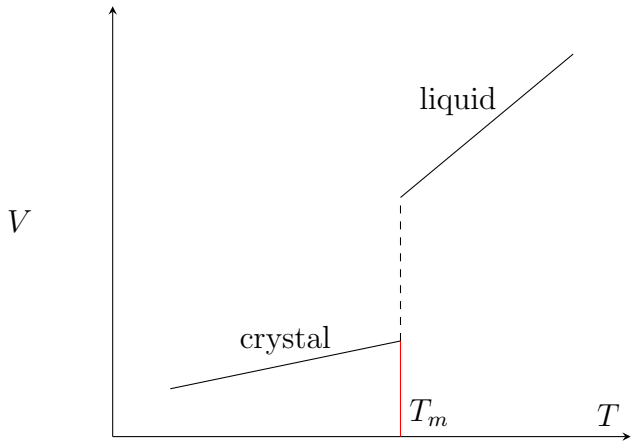

Figure 3.8: Specific volume V vs temperature T of a polymer under melting or crystallization.

In amorphous regions, materials stay in the form of a disordered liquid (viscous or rubbery) at temperatures above T_g, and transform into a disordered solid below T_g [48]. At

the glass transition temperature T_g, the specific volume of the material evolves continuously, and there is no latent heat involved. The physics of glass transition has not been fully understood yet, and controversy exists in describing this process. It is claimed in some theories [49] that glass transition is a second-order phase transition, although some people consider it as a purely kinetic process [50]. Although there is no latent heat, the heat capacity of the sample does change, as indicated by the slope change in Figure 3.9. One thing to note is that the glass transition normally occurs in a range of temperatures, rather than at a single point, and it always occur below T_m. This is because the glassy state is not a thermodynamically-stable state, and the measurement of T_g depends on factors such as the polymer's thermal history and the heating or cooling rate.

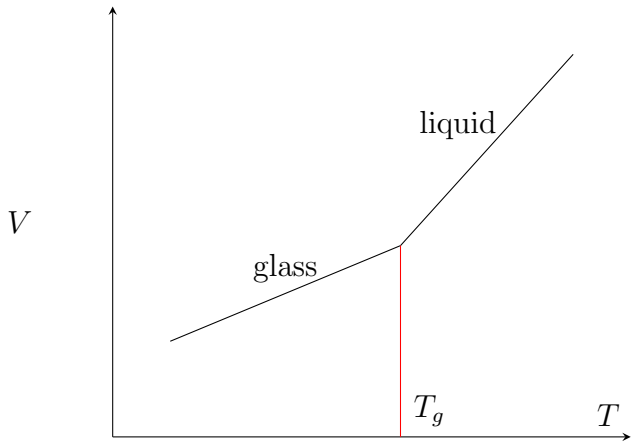

Figure 3.9: Specific volume vs temperature of a polymer under glass transition, where T is the temperature and V is the specific volume.

One major difference between first-order and second-order phase transitions is their driving force. In a melting transition, the process is driven by thermodynamics, as the crystalline state is the thermodynamic ground state at low temperatures. However, the glass state is not a ground state, with the chains not being fully ordered. It has been suggested in some theoretical predictions that given long enough relaxation time, the glassy state would finally transforms into the crystalline state [51]. Instead of being thermodynamically driven, the glass transition is normally considered as a kinetic transition.

3.3.2 Working mechanism of differential scanning calorimetry

Differential scanning calorimetry (DSC) is an instrument that measures the heat flow to the sample material within a controlled temperature range. Inside a typical DSC there are two metal (Al commonly) pans, with one acting as the sample pan and another empty pan acting as a reference. Through precise heating and cooling control with a feedback mechanism, the two pans are maintained at the same temperature at any time during the scanning measurement. At temperatures where phase transitions of the sample material takes place, the heat capacity of the sample changes, which requires the computer to adjust the amount of heat flow provided, in order to always keep the two pans at the same temperature. The heat flow $\frac{dQ}{dt}$ is obtained as a function of temperature, which depends both on the heat capacity C_p of the sample and the scanning rate q:

$$\frac{dQ}{dt} = \frac{dQ}{dT} \cdot \frac{dT}{dt} = C_p q \tag{3.12}$$

By plotting the difference between the heat flows to the two pans with respect to temperature, thermal transitions that the sample material experienced during the set range of temperature, such as crystallization, melting, and glass transition, can be determined. Figure 3.10 is a typical DSC curve. When the scanning rate is constant, first-order transitions appear as peaks on the DSC curve. Crystallization appears as an exothermic peak on the cooling curve, and melting appears as an endothermic peak on the heating curve. The difference observed between the crystallization temperature T_c and the melting temperature T_m is supercooling ΔT.

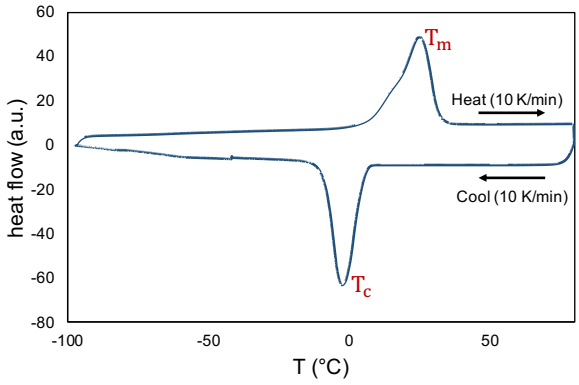

Figure 3.10: DSC curve for the neat sample before evaporation.

3.4 Results from differential scanning calorimetry

The products previously pressed into Al pans were characterized with a DSC machine (Q100, TA Instruments). The following running process was performed on each product: equilibrate at 353 K (to fully melt all crystal); isothermal for 5 min; ramp 10 K/min to 173 K (to crystallize the sample); isothermal for 5 min; ramp 10 K/min to 353 K; isothermal for 5 min; ramp 10 K/min to 173 K; isothermal for 5 min; ramp 10 K/min to 353 K. With two runs of the same procedure, we examined the reproducibility of the results.

3.4.1 Melting temperature

From the DSC curves of each fraction, we noticed that most of the samples show a double-peak pattern, with a lower T_{m1} and a higher T_{m2}, as shown in Figure 3.11. We then determined each melting temperature of every fraction, as plotted in Figure 3.12. Each measurement was carried out more than once, and the T_m values from separate measurements normally varied within $\pm$ 2 degrees. $\bar{N}$ is the average N value of each sample, which was interpolated linearly based on the 10 samples measured with MALDI. In general, the

melting temperatures behave as described by the Gibbs Thomson relation, with the higher N values (longer chains) showing higher melting temperatures.

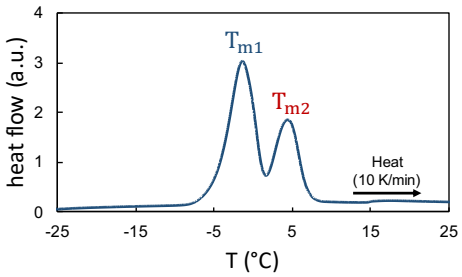

Figure 3.11: Double-peak pattern observed on the DSC heating run of a purified fraction.

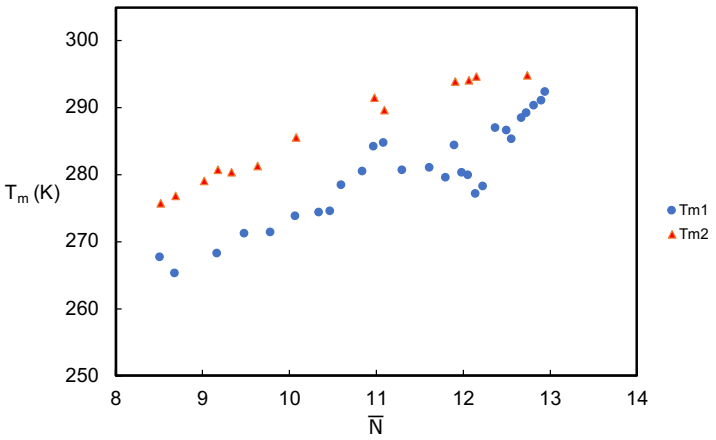

Figure 3.12: Melting temperature of purified fractions.

Chain-folding analysis based on T_m

In Figure 3.12, it is obviously seen that the data points potentially lie on two roughly parallel curves, which brings our assumption that they could correspond to two types of chain-folding modes in the crystal lamellae, with the higher T_m's being extended chains (larger thickness), and the lower T_m's being once-folded chains (smaller thickness).

In order to validate our assumption, we apply Equation 3.9 to see if we are able to get a good fit with the two series of data. Parameters for PEO present in this equation, including T_m^∞ [7], V [52], ΔH [53] are found in the literature. Interfacial tension S is dependent on the mode of chain-folding, as both chain ends and chain folds contribute to the amorphous phase, and they lead to different interfacial tensions with respect to the crystalline phase.

The interfacial tension of chain folds, S_{folds}, can be obtained from parameters of PEO chains with large molecular weights. This is because in the crystal lamellae of long chains, the number of chain folds are much greater than that of chain ends, and thus S is dominated by chain folds. For long PEO chains, crystal lamellar thickness L is normally on the order of 10 nm [54], and the melting temperature of high molecular weight PEO is around 65°C [55]. With the other parameters previously found, we are able to calculate $S_{folds} = 98.4 mJ/m^2$ from Equation 3.9.

However, to quantitatively look at the thermodynamics of extended chains and once-folded chains in our assumption, and to fit the Gibbs Thomson relation of these two modes to our data, we need to know the actual interfacial tensions in these two modes.

For extended chains, the interfacial tension S_{ext} merely comes from chain ends, while for once-folded chains, apart from the chain ends, there are also chain folds that contribute to the interfacial tension S_{1-fold}. S_{ext} and S_{1-fold} can be obtained by adjusting their values based on S_{folds} (previously calculated for long chains). The reason we are able to do this is that even though they arise from different parts in the polymer, the interfacial tension between crystalline and amorphous regions should not vary significantly (at least on the same scale) for a certain polymer. The following two figures and illustrations describe how we achieved our fitting and established our model on the conformation of chains.

For extended chains, we fit the higher melting points with the Gibbs Thomson equation, using the value of S_{folds} initially, and then adjust its value until we get a good enough fit (Figure 3.13). This value is then taken as $S_{ext} = 275.1 mJ/m^2$.

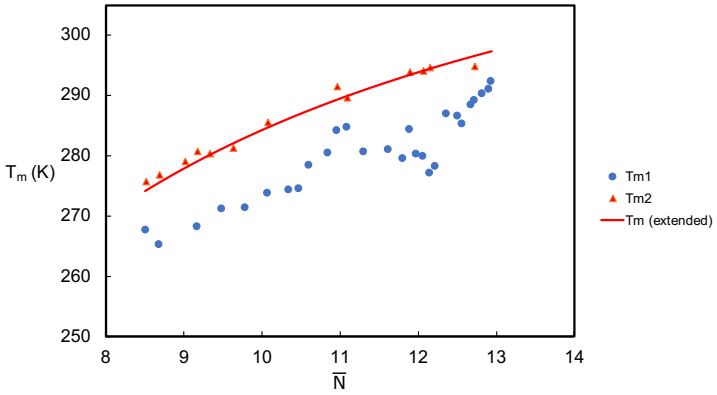

Figure 3.13: T_{m1} data fitting to Gibbs Thomson equation.

For the lower melting points, which correspond to once-folded chains, the chains emanating from the lamella enter the amorphous phase to make a fold, and then re-enter the lamella, where 3.5 monomers are needed for a single chain to complete this turn, as introduced in Section 3.2.1. This conformation then has two chain-end monomers on one side of the lamella, and 3.5 monomers on the fold on the other side, which enables us to calculate the interfacial tension S_{1-fold} as:

$$S_{1-fold} = \frac{2S_{ext} + 3.5S_{folds}}{2 + 3.5} = 162.7mJ/m^2 \tag{3.13}$$

With every parameter in the Gibbs Thomson equation obtained, we then generated the curve of melting temperature of once-folded chains as a function of N values. The good agreement between the curve and the real data points (Figure 3.14) suggests that this is a possible and reasonable model of chain conformation.

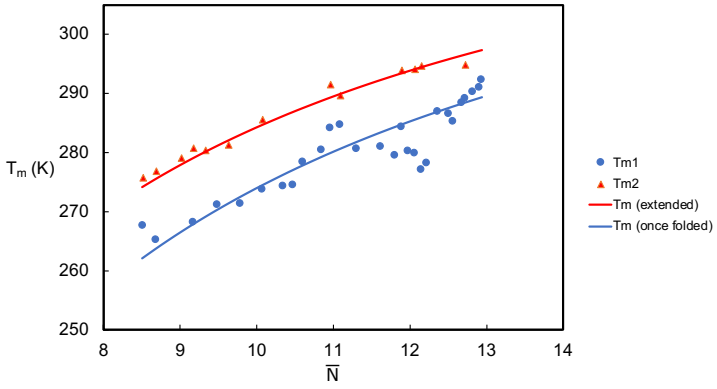

Figure 3.14: T_{m1} and T_{m2} data fitting to Gibbs Thomson equation.

In the plots of melting temperatures, the x-axis, $\bar{N}$, is the number average value of all the composing N's in each fraction, characterized directly with MALDI or interpolated based on the MALDI data. However, only with single integer N values could we be able to talk about the melting temperatures given by the Gibbs Thomson curves. For a mixture of different N's, its melting temperature potentially lies anywhere within the range of T_m's of its composing N's. A more careful way to present our chain-folding models together with the T_m data would be as Figure 3.15 shows. Dashed boxes are generated for each T_m curve, with the top (bottom) of the box representing the melting point of the highest (lowest) N value present in any potential purified fraction lying on the curve in this particular box. In generating the bars, N components with a percentage less than 5 % are neglected. Notice that each curve passes through all of the corresponding boxes, with only a few data points falling outside.

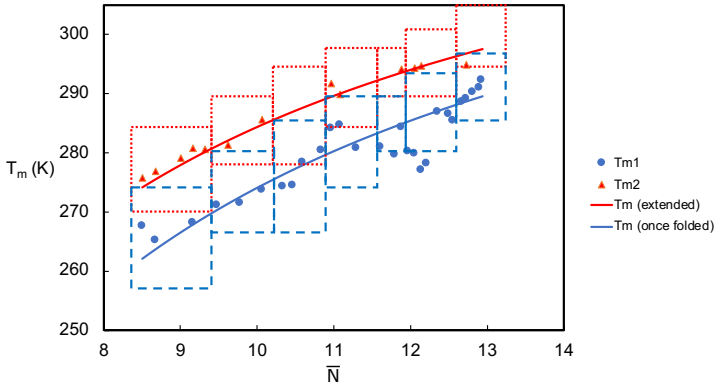

Figure 3.15: Gibbs Thomson relation fitting with potential range bars on T_m data points.

Comparison to N-alkanes

As mentioned previously, PEO is a polymer with linear structure, as well as N-alkanes and polyethylene. Therefore, some comparisons to N-alkanes are necessary to better understand the phenomena and properties we have observed.

Before the lamellar structure of PEO was discovered, N-alkanes had been revealed to form "single crystal platelets", with the chain ends at the surface of these lamellae [56]. The thickness of each lamella was around 100 Å, while it could vary from 60-80 Å to up to 150 Å, depending on certain conditions [57]. In order for long chains whose extended length was larger than this thickness to fit in such a layer, polymers were found to fold back and forth in the layer. Depending on the length of chains, they needed to fold for different times in the lamellae. For N-alkanes, the lower molecular weight limit for fold-chain conformation was 2100 g/mol, or 150 carbon atoms in the chain [58]. For crystallization from solutions, this limit was slightly lower than that from the melt, but still similar [13].

It was further discovered that for long N-alkanes, the fold length (lamella thickness) was a function of crystallization temperature T_c. When the supercooling was small, lamellae grew with larger thickness [58].

The number of folds for each polymer chain was at first believed to be quantized, i.e., the chains could only take integer number of folds in the lamella, or they existed as

extended chains [58]. Kovacs *et al* obtained same results for PEO oligomers as well, where only integer folds were allowed [42]. However, it was later discovered that non-integer folds (NIF) were also possible. Real-time small-angle X-ray scattering (SAXS) experiments [59] revealed that at early stages of crystal formation, long alkane chains formed NIF crystals. The amorphous layers in between of lamellae of NIF crystals had a thickness of 6 to 8 nm, which were much looser than those of extended chain crystals. During crystallization, NIF lamellae further thickened or thinned until the thickness reached integral fractional (IF) values of the extended chain length, through refolding of chains. The amorphous layers then became denser and the folds turned sharper, corresponding to a more stable state of the crystal [58].

Richardson [56] studied single crystal polyethylene with an adiabatic calorimeter, in order to investigate the folding and chain re-entry in the lamellae. Chains exiting the crystalline layer might return to themselves immediately, as suggested in the adjacent re-entry model in Section 3.1.1, or they might float in the amorphous region, and return to the lamellae from a further site, resulting in a loose fold. From the result of calorimetry and small-angle X-ray experiments, the number of carbon atoms involved in each sharp fold in the adjacent re-entry model was found to be six, which is three monomers for polyethylene. For low molecular weight PEO, the number of monomers on a fold is 3.5 on average, which is comparable with polyethylene.

Fractionation of chains during crystallization

In the DSC measurements, fractionation of chains with different N's is sometimes observed. During some of the repeated DSC measurements, several samples showed double melting peaks (an example shown in Figure 3.16), with both melting temperatures near the same T_m curve. The two peaks were separated by around 3 K, which is likely the difference between the melting temperatures of two neighbouring N's according to our calculation, rather than the difference between the two chain conformations (extended and folded). It is worth noting that this fractionation is more commonly observed at the higher T_m than at the lower T_m, because in the extended conformation, the crystal lamellae composing of

two neighbouring N's have a larger difference in thickness than in the folded conformation.

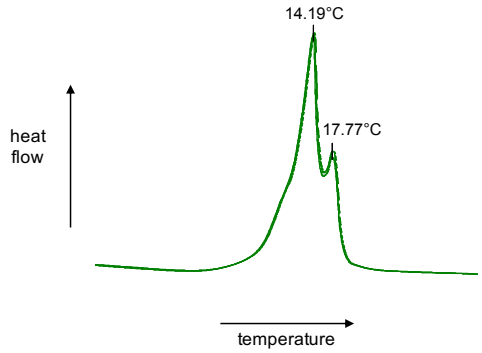

Figure 3.16: Part of DSC curve (melting) from regular run on $\bar{N} = 11$.

Tuning chain-folding mode

Most of the fractions showed two melting points in DSC measurements, while some of the fractions only showed one, lying either on the T_{m1} curve or the T_{m2} curve. For the fractions where the higher T_m was observed, on the DSC cooling ramp usually showed two crystallization peaks, suggesting that the polymers still formed both extended and folded chain structures, but before increasing to the melting temperature, once-folded chains relaxed themselves and recrystallized into extended form. However, when the lower T_m was present, only one crystallization peak was observed on the This is an indication that the cooling rate during crystallization might not have been slow enough for the chains to crystallize in the extended form.

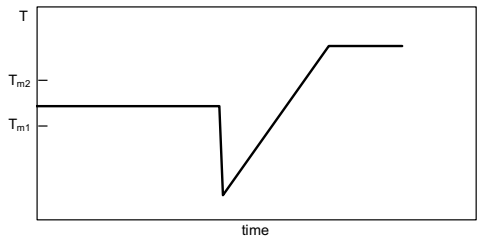

Figure 3.17: Thermal treatment on products with a lower T_m present.

The following treatment (as shown in Figure 3.17) was then applied to further verify our observation. With some of the fractions that showed the lower T_m (either with or without the higher T_m) in normal DSC measurements, we kept the sample at a temperature between T_{m1} and T_{m2} for a time long enough to melt all the once-folded chains and leave all the extended chains. Then we quickly cooled the sample to a much lower temperature, and measured its melting again. During the second DSC measurement only the higher T_m appeared, which was a direct validation that we had successfully forced the once-folded chains to recrystallize into extended chains by applying the treatment. Figure 3.18 is an example measurement we did on a purified fraction with $N = 12.3$. This treatment and the result we obtained is again a proof of the existence of folded chain configurations in the crystal lamellae. However, as introduced previously, PEO chains have been believed to fold only when $N \geq 45$. Therefore, this is a surprising result to us, and further investigations are needed to reveal the mechanism behind it.

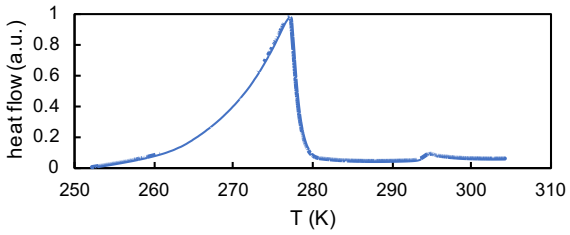

(a) Before thermal treatment there is a major melting transition peak followed by a small peak.

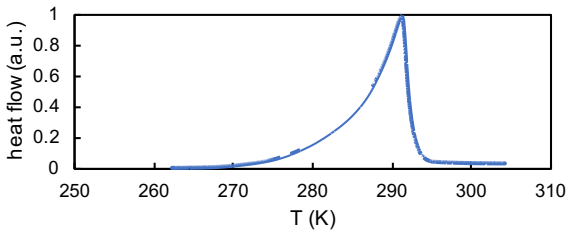

(b) After thermal treatment only one melting peak near T_{m2} is observed.

Figure 3.18: DSC measurements on a purified fraction with $N = 12.3$ before and after thermal treatment.

Comparison between purified fractions and neat sample

When we compared the DSC curves of the neat sample and the purified fractions, some of the fractions showed unexpected melting behaviours (Figure 3.19). From the curves of some products obtained at early stages of evaporation, the neat mixed sample should start melting at temperatures much lower than the observed melting temperature of the neat sample. However, this was not observed. Instead, we believe that when the short chains are mixed with longer chains, they become influenced and crystallizes differently than in a more monodisperse sample. One of the possible explanations to this is that in the presence of longer chains, the shorter chains tend to act as the amorphous phase, even at temperatures lower than their own melting points. It is also possible that the short chains only represent a very small portion (fractions with $N \leq 10$ are 14% of the neat sample) of the neat sample. Therefore the heat flow signal from them could easily be overwhelmed by that of major components.

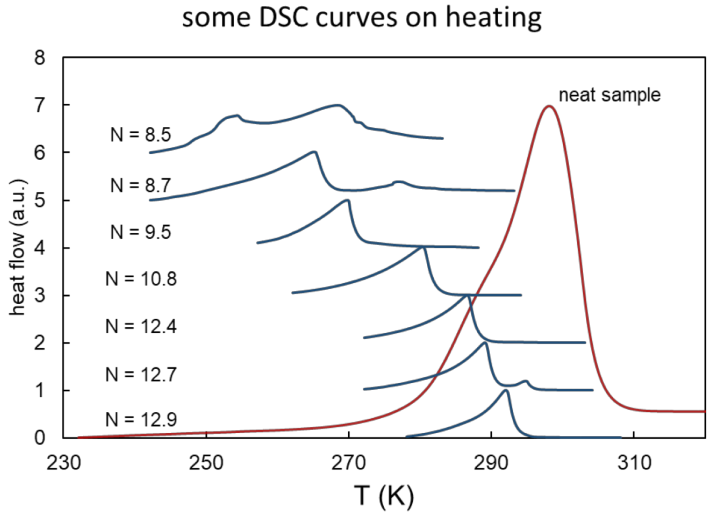

Figure 3.19: DSC curves of the neat sample (red) and some of the purified fractions (blue).

End-group effects

In 3.2.2, we reviewed Yeates' study on the melting of monodisperse and polydisperse PEO oligomers. Now we would like to compare our results for purified fractions with theirs. Surprisingly, it turns out that the melting temperatures we obtained agreed more with the polydisperse samples in their measurements. This could be an indication that the melting points difference they observed between the monodisperse and polydisperse samples is very unlikely to be due to polydispersity. Instead, it could be related to specific properties such as end-group chemistry.

End-group effects on PEO crystallization has been studied by many researchers and it has been found that the type of end-group directly influences properties including melting temperature and crystallinity, as shown in Table 3.1 [60]. Monodisperse PEO with hydroxy end-groups has been reported to display different crystallinities and T_m's than that with methoxy end-groups. The difference in crystallinity is believed to be due to different heats of interaction related to the end-groups at the lamellar surfaces. The difference in melting temperature is attributed to different environments at a crystalline lamellar surface and in melt, because lamellar surfaces are much more ordered compared to the melt, which magnifies the effect of end-groups on the surfaces, while in a melt, the effect of end-groups could be hidden in the melt background. Polydisperse PEO samples with different end-groups, however, display different crystallinities but similar T_m's. It is argued that rejection of methoxy end-groups from the lamellar surfaces results in higher entropy of the crystal, leading to a lower enthalpy of melting, and a lower crystallinity. In terms of the melting temperature, it is claimed that the disordered lamellar surface and the melt have similar environments, so the effect of end-groups on T_m's would appear less significant.

	monodisperse PEO	polydisperse PEO
crystallinity	different	different
T_m	different	similar

Table 3.1: Comparison of PEO with hydroxy and methoxy end-groups (reproduced from [60]).

In our experiments, the PEO samples only contain hydroxy end-groups, while in Yeates' study, the synthesis of monodisperse samples involved end-groups containing sulfur. Based on the evidence and analysis mentioned above, the disagreement between our results and theirs could be that sulfur results in different interaction energy with the crystalline layer, and potentially led to different melting temperatures. Sulfur has been found to decrease the interfacial tension of liquid iron with Al_2O_3 [61], and also decrease the interfacial energy between Fe-C melt and graphite [62]. However, no direct measurement results have been found in terms of the effect of sulfur-containing end-groups on the interfacial energy and melting temperature of a polymer.

3.4.2 Degree of crystallinity

PEO has been known as a polymer with high crystallinity due to its linear structure. However, based on the fact that polymers almost never crystallize completely, it is of interest to study the degree of crystallinity X_c of our samples. We determined X_c of the products from the heat of fusion $\Delta H_f(T_m)$ on melting in DSC measurements. The heat of fusion can be calculated from the area under the melting peak, and the degree of crystallinity was defined as [53]:

$$X_c = \frac{\Delta H_f(T_m)}{\Delta H_f^0(T_m^0)} \tag{3.14}$$

where X_c is the degree of crystallinity by weight fraction, $\Delta H_f(T_m)$ is the enthalpy of the melting transition, and $\Delta H_f^0(T_m^0)$ is the enthalpy of melting of PEO with 100 % crystallinity [53]. By integrating the melting peaks on the DSC curves, we obtain X_c of the purified products, as shown in Figure 3.20.

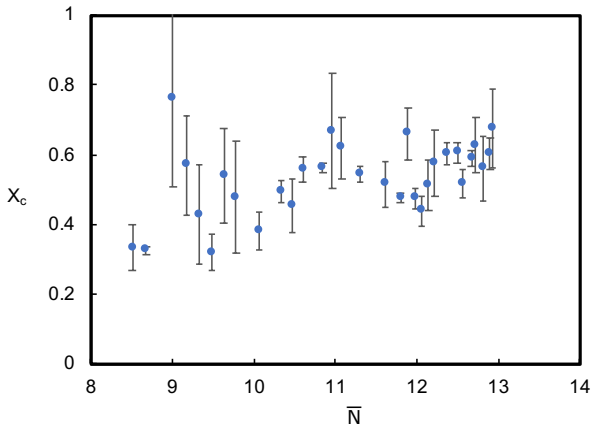

Figure 3.20: Degree of crystallinity of purified products.

It is easily noticed from the figure that our data is not precise enough since the error bars for some of the fractions are quite large. This results from the deviation (0.1 mg) of the scale used to weigh the samples. The enthalpy of melting $\Delta H_f(T_m)$ calculated from the DSC curve is directly related to the weight of sample, and for samples with a small weight, the deviation is comparable to its weight. Therefore, for more precise measurement of X_c, larger amounts of sample are required, which brings forward the demand for technical improvements including scaling-up of our evaporative purification system.

We would also like to compare our results of PEO crystallinity with other studies, as shown in Figure 3.21. Although there are a limited number of measurement results on PEO crystallinity with such low $\bar{N}$ values, most of our results lie in the range of several other studies in the literature.

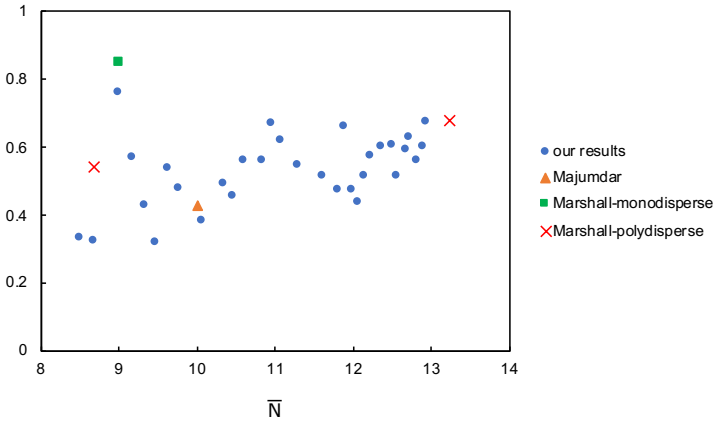

Figure 3.21: Comparison of degree of crystallinity measured in different studies. Majumdar: data from "Physical characterization of polyethylene glycols by thermal analytical technique and the effect of humidity and molecular weight" by R Majumdar *et al*, *Pharmazie*, 65:343-347, 2010 [63]. Marshall: data from "Crystallinity of Ethylene Oxide Oligomers" by A Marshall *et al*, *Eur. Polym. Journal*, 17(893), 1981. [60].

An interesting fact about the X_c data is that when we bring Figure 3.20 and Figure 3.12 into comparison (even though X_c and T_m are not directly related), it was noticed that they have a similar trend, especially with the bump pattern located at $\bar{N}$ around 11. However, the reason behind this observation is still unclear to us and needs further investigation.

Chapter 4

Crystal growth review and measurements

In the previous chapter we discussed the thermodynamics of polymer crystallization, while this process is in fact controlled by kinetics more than thermodynamics due to the nature of polymers. Kinetic theories typically analyze a process from two aspects: "driving force" and "free energy barrier" [36]. "Driving force" in the case of polymer crystallization refers to the free energy difference between the crystalline state and the amorphous state, and "free energy barrier" includes all kinds of factors that are against the crystallization process, such as entanglement of chains, defects in the system, etc. These two factors compete with each other, and the system reaches the most stable state by balancing them.

4.1 Crystallization with spherulites

When a polymer crystal is grown from a melt, superstructures called spherulites are normally formed. These structures are composed of stacked lamellae that have grown from a common centre, as shown in Figure 4.1. Spherulites are normally formed when there is no thermal gradient present, because in the presence of thermal gradient with a certain direction, crystal growth would follow the gradient instead of growing radially [3]. In spherulites,

polymer chains are aligned perpendicular to the radius of the spherulite. During crystallization, the spherulites grow until they contact each other, and their sizes range from microns to millimeters [64], which can be easily observed under an optical microscope. Among the crystalline stacks are amorphous regions, together forming a semicrystalline structure.

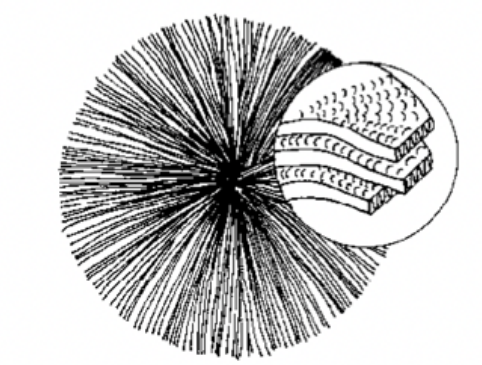

Figure 4.1: A polymer spherulite with folded-chain lamellae. Figure source: "The Morphology of Crystalline Synthetic Polymers" by F. Khoury and E. Passaglia, *Treatise Solid State Chem.*, pages 335–496, 1976 [65].

The growth of a spherulite is controlled by many factors including the number of nucleation sites, polymer structure, crystallization temperature, cooling rate, etc. For example, if the crystallization temperature is low enough or there are a large number of present nuclei, many spherulites would be created and grow into relatively small sizes; while if the supercooling is small, and fewer nuclei are present, fewer spherulites would form, but they would be larger in size [66]. Spherulites are optically anisotropic because of the alignment of the linear polymer chains. When they are viewed under an optical microscope, with crossed polarizers on, certain patterns such as the "Maltese cross" consisting of eight alternating bright and dark fan-shaped areas (Figure 4.2) are often observed, resulting from the birefringence of the lamellae [67].

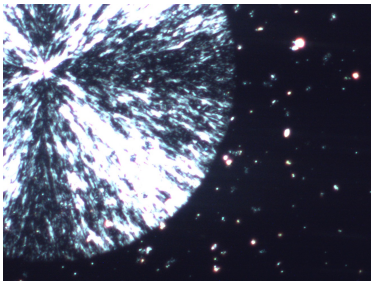

Figure 4.2: Optical microscope image (with crossed polarizers on) of fraction with $\bar{N} = 12.4$ at 260.65 K.

4.1.1 Nucleation

Crystallization can be divided into two stages: nucleation and crystal growth. Nucleation is the primary step in the crystallization of a polymer. As temperature decreases, a polymer normally does not crystallize immediately when it reaches the melting temperature, but rather needs a considerable supercooling before crystallization. The reason is that crystallization starts with nucleation, and if the polymer sample has little or no nuclei present, the temperature is able to kept decreasing until the sample grows a nucleus from itself, which is called primary nucleation. The driving force of this process is the local density fluctuation, and it is able to occur at temperatures below the melting temperature and above the glass transition temperature.

Apart from primary nucleation, there are also secondary and tertiary nucleation. If we consider the formation of a cubic nucleus, primary nucleation requires 6 new faces to be formed, while secondary nucleation requires 4 new faces (on the surface of present nuclei), and tertiary nucleation requires only 2 new faces (at the edge of present nuclei) [11].

Primary nucleation is further classified into homogeneous nucleation and heterogeneous nucleation. Homogeneous nucleation refers to a nucleation process that is purely induced by thermal fluctuations and does not involve the influence of any solids, including present crystal, container walls, or foreign particles present in the crystallizing sample. Heterogeneous nucleation, however, refers to a primary nucleation with the help of impurity

particles, either uncontrolled or deliberately introduced into the sample [21]. Homogeneous nucleation will be mainly focused on here, but heterogeneous nucleation is much more common in real cases. Foreign particles help greatly reduce the free energy barrier of the phase transition from liquid to crystal, and lead to a smaller supercooling.

In a homogeneous nucleation process, thermal fluctuations result in the formation of embryos (small aggregates with enhanced inner order), and the size of the embryos determines if they could survive through the energy barrier and grow into a larger crystal. If the embryo is not big enough, there would only be a small free energy loss caused by crystallization, compared to the free energy barrier in creating their surfaces. In this case, the embryo can not survive and would have to melt. Assuming the embryos are spherical, the classical nucleation theory can be applied to derive the critical size of an embryo [11].

The total free energy of an embryo is:

$$\Delta G = -\frac{4}{3}\pi r^3 \Delta g + \sigma_e 4\pi r^2 \tag{4.1}$$

where r is the embryo radius, Δg is the free energy per unit mass on melting, and σ_e is the surface free energy of the embryo.

The plot of ΔG vs r is shown as Figure 4.3. We note that there is a maximum in ΔG, ΔG^*, for a critical r value, r^*. Below this value, ΔG increases with r, while after surpassing it, ΔG decreases as r increases. When the thermal fluctuations are strong enough to produce embryos larger than r^*, the embryos could then grow into crystals. These two critical values can be calculated [68] from Equation 4.1 by differentiating ΔG and equating to zero:

$$r^* = \frac{2\sigma_e}{\Delta g} \tag{4.2}$$

$$\Delta G^* = -\frac{16\pi\sigma_e^3}{3\Delta g^2} \tag{4.3}$$

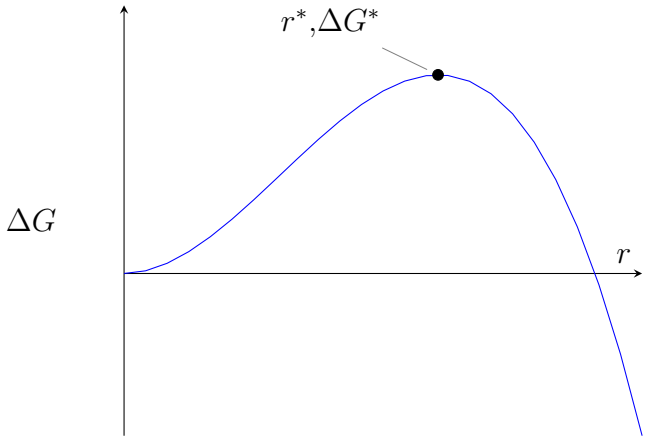

Figure 4.3: Total free energy of an embryo ΔG vs embryo radius r, where r^* and ΔG^* are the critical radius and the critical free energy, respectively.

Intuitively we would expect both r^* and ΔG^* to show a negative correlation with the extent of supercooling ΔT, and in fact this can be proved as follows. Assuming that the enthalpy and entropy do not vary significantly near the crystallization temperature, we obtain:

$$\Delta g(T_m) = \Delta h(T_m) - T_m \Delta s(T_m) = 0 \tag{4.4}$$

$$\Delta g(T_c) = \Delta h(T_c) - T_c \Delta s(T_c) = 0 \tag{4.5}$$

Equations 4.4 and 4.5 can be rearranged into Equation 4.6:

$$\Delta g(T_c) = \Delta h(T_c) - T_c \frac{\Delta h(T_c)}{T_m} = \Delta h(T_c) \frac{T_m - T_c}{T_m} = \Delta h(T_c) \frac{\Delta T}{T_m} \tag{4.6}$$

Within the context of the case of embryo growth, Equation 4.6 can be modified to yield Equation 4.7:

$$\Delta g = \Delta h \frac{\Delta T}{T_m} \tag{4.7}$$

Taking advantage of the relationship between Δg and r^* in Equation 4.2 and ΔG^* in Equation 4.3, Equation 4.8 and 4.9 could be derived:

$$r^* \propto \Delta T^{-1} \tag{4.8}$$

$$\Delta G^* \propto \Delta T^{-2} \tag{4.9}$$

As the crystallization temperature (T_c) gets lower, corresponding to a larger supercooling ΔT, r^* and ΔG^* get smaller, indicating an easier nucleation. In addition, according to the nucleation theory by Turnbull and Fisher [69], the nucleation rate, i, is expressed as:

$$i = i_0 exp(-\frac{\Delta E + \Delta G^*}{kT}) \tag{4.10}$$

where i_0 is a pre-exponential factor, ΔE is the nucleation activation energy, and ΔG^* is the critical nucleation energy. The dependency on ΔT through ΔG^* suggests that the nucleation rate i is higher for a larger supercooling, and thus a faster nucleation. However, we need to be careful that when temperature decreases to near the glass transition temperature, T_g, chain mobility is highly restricted, which makes it harder for thermal fluctuations to produce nuclei. Therefore, there exists a maximum nucleation rate at a temperature between T_g and T_c.

Nucleation can be described by the nucleation time τ_{nuc} as well, which is simply the inverse of the nucleation rate, and can be directly measured. The nucleation rate is significantly slower than the crystal growth rate, especially for homogeneous nucleation, which makes it very convenient to measure the rate of these two processes separately. In a study [70] of homogeneous nucleation in PEO crystallization, the relationship between τ_{nuc} and the volume of the crystallizable droplets V was shown. Impurity-free discrete PEO droplets are formed through dewetting on a polystyrene film, and cooled under an optical microscope with crossed polarizers to observe the nucleation of each droplet. Figure 4.4 presents their findings.

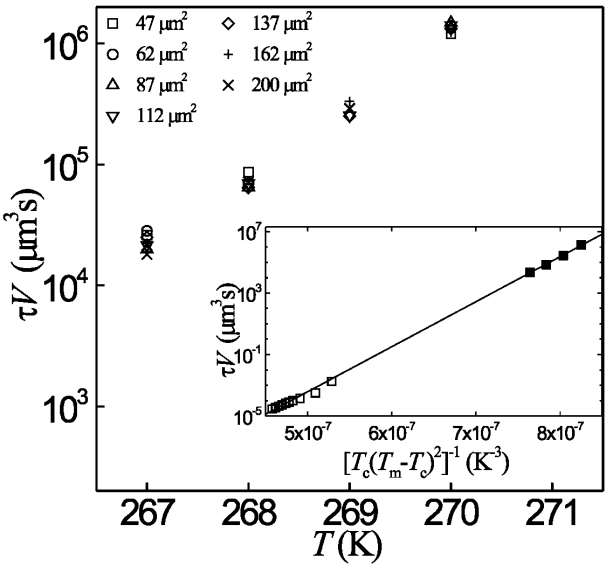

Figure 4.4: Volume-normalized time constant, τV, as a function of temperature. In the index the averaged dewetted droplet data (solid symbols) are in agreement with data from [71] (open symbols), both with linear dependence on $[T_c(T_m - T_c)^2]^{-1}$ as expected from classical nucleation theory [21]. Figure source: "Homogeneous Crystallization of Poly(Ethylene Oxide) Confined to Droplets: The Dependence of the Crystal Nucleation Rate on Length Scale and Temperature" by Michael V. Massa *et al*, *Phys. Rev. Lett.*, 92(25):255509, jun 2004 [45].

The observation results show that τ_{nuc} is inversely proportional to the volume as shown in Equation 4.11:

$$\tau_{nuc} \propto V^{-1} \tag{4.11}$$

At the same crystallization temperature, droplets with different volumes have the same value of the volume-normalized time constant, τV, and it decreases (meaning increasing rate) exponentially as the supercooling becomes larger. The close agreement between these two sets of data and their huge difference ($\sim$ 8 orders of magnitude) in τV suggests that the nucleation mechanism is consistent within a huge range of size. The many differences in these two experimental systems indicates that nucleation is dominated by the bulk rather

than the surface.

4.1.2 Crystal growth

After nuclei have been formed, the ones with radii larger than r^* can grow into larger crystals by adsorbing crystallizable materials. Crystal growth is either diffusion-controlled or interface-controlled.

Crystals growing from dilute solutions are typically diffusion-controlled, since in such cases the growth rate depends on the diffusion rate of the crystallizable material onto the surfaces of nuclei. According to Fick's diffusion law [72, 73], the relationship between the radius of a crystal r and time t has been found to be well-represented by Equation 4.12 [74, 75, 76, 77]:

$$r \propto t^{\frac{1}{2}} \tag{4.12}$$

When the solution concentration is high, or when the crystal is growing from a melt, the diffusion rate is no longer the limiting factor in its growth, because the nuclei are surrounded by sufficient crystallizable materials. Therefore, it depends more on the attachment of crystallizable material onto existing nuclei. The attachment and the formation of crystal lamellae are well-described by the widely-accepted theory proposed by Lauritzen and Hoffman [78, 79, 80]. The theory relates microscopic movements to macroscopic quantities, and has become the most successful theory to describe this process, although it has also been criticized by some researchers saying that it oversimplifies crystal growth by applying a mean field description [36].

Lauritzen-Hoffman (LH) theory treats crystal growth as a secondary nucleation process, and one of the basic assumptions is that the nucleus is in fact a single stem grown from thermal fluctuations. It then acts as a growth front, and other stems deposit onto its surface and crystallize stem by stem into a lamella, thus creating a new layer through lateral spreading. When the present surface layer is taken up, this spreading process is repeated if another nucleus is formed on top of this layer.

In order to quantify this process, four parameters need to be defined: the surface nucleation rate, i; lateral covering rate, g; perpendicular growth rate, G; the length of surface, L. Three regimes are predicted in the model, as shown in Figure 4.5.

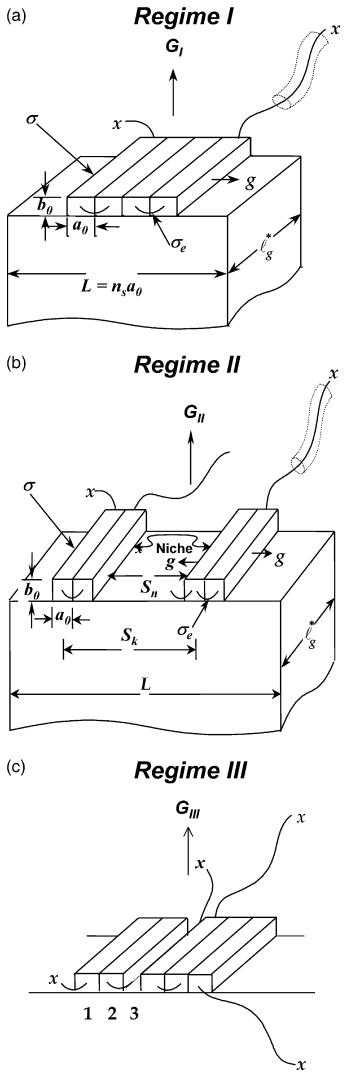

Figure 4.5: Polymer crystal growth in three regimes in LH theory. Figure source: "Enthalpic and entropic origins of nucleation barriers during polymer crystallization: the Hoffman–Lauritzen theory and beyond" by Stephen Z.D. Cheng *et al*, *Polymer (Guildf).*, 46(20):8662–8681, sep 2005 [81].

In regime I, ΔT is low, and according to the nucleation theory [69] mentioned in 4.1.1, the nucleation rate i is low. In the case where i is smaller than g, there is enough time for polymer chains to cover the entire surface, since this process is restricted by i. The crystal growth rate G_I in this regime is given by Equation 4.13:

$$G_I = ib_0L \tag{4.13}$$

where b_0 is the thickness of the new layer formed. LH theory describes that after nucleation (rate-controlling process) takes place, new stems cover the surface by fast lateral growth, and form a new growth front awaiting the next round of nucleation.

As T_c decreases, ΔT increases, and the crystal growth reaches regime II, where i is now comparable to g, and multiple nuclei could be formed at the same time. The growth rate is then dependent on both i and g:

$$G_{II} = (ib_0g)^{\frac{1}{2}} \tag{4.14}$$

In this regime, the surface is less smooth than that in regime I, since multiple nuclei are present when new stems crystallize onto the surface.

At even lower T_c, ΔT keeps decreasing, and the crystal growth reaches regime III, where i becomes larger than g, and the separation between two neighbouring nuclei decreases to be comparable to the stem width, so the chains could quickly cover the surface. In this case, the crystal growth rate is again dominated by i:

$$G_{III} = ib_0L' \tag{4.15}$$

where L' is the separation between neighbouring nuclei, which is normally about 1-3 stem widths [82]. Neighbouring nuclei are so close to each other that the lateral growth rate, g, is not significant in this regime. The crystal surface is even rougher than that in regime II.

As previously mentioned, LH theory treats crystal growth as a secondary nucleation process, and thus the crystal growth rate should have a similar dependence on temperature as the nucleation rate does. Figure 4.6 shows the dependence of the growth rate on temperature for spherulites of isotactic-polystyrene, poly(ϵ-caprolactam) (nylon) and poly(tetramethyl-*p*-silphenylene siloxane) (TMPS). The maximum growth rate occurs at a temperature between the glass transition temperature T_g and the melting temperature T_m, as expected from the nucleation process.

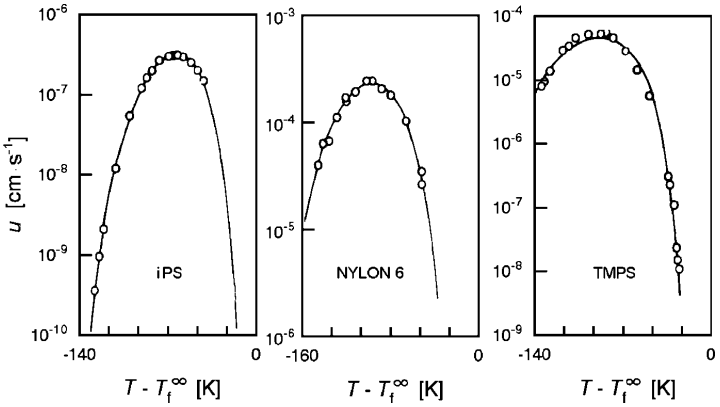

Figure 4.6: Temperature dependence of the radial growth rate u of spherulites of iPS, nylon and TMPS. Figure source: "Nucleation and Crystallization" by Gaylon S. Ross *et al*, *Methods Exp. Phys*, 16:339–397, jan 1980 [83].

4.2 Review of PEO oligomers crystal growth rate

The crystal growth rate of PEO oligomers, the polymer investigated in this thesis, has been investigated by many researchers. One of the earliest and most famous studies was done by Kovacs *et al* [32]. Figure 4.7 and Figure 4.8 show the growth rates vs temperature and molecular weight.

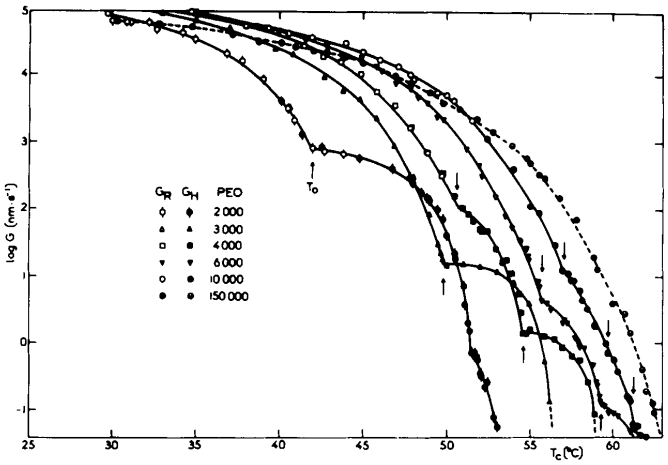

Figure 4.7: PEO crystal growth rate with respect to temperature and molecular weight. Figure source: "Isothermal growth, thickening, and melting of polyethylene oxide) single crystals in the bulk" by A J Kovacs *et al*, *J. Polym. Sci. Polym. Symp.*, 50(1):283-325, 1975 [32].

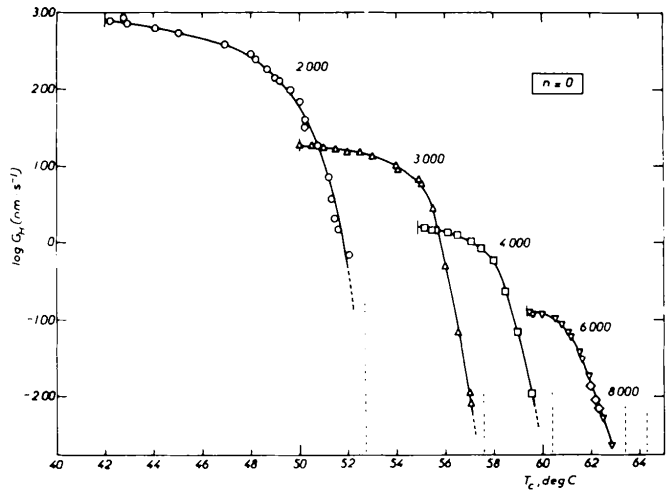

Figure 4.8: Extended-chain PEO crystals growth rate with respect to temperature and molecular weight. Figure source: "Isothermal growth, thickening, and melting of polyethylene oxide) single crystals in the bulk. II" by A J Kovacs *et al*, *J. Polym. Sci. Polym. Symp.*, 59(1):31–54, 1975 [42]

.

Two types of growth rates were measured in their study. G_R refers to the radial growth rate of spherulites, and G_H, or $G(010)$, refers to the radial growth rate along the (010) prism faces. For the measurement of G_R, several low molecular weight PEO samples were sandwiched between cover slips, forming films about 10 µm in thickness, and crystallized at different temperatures. The growth rates of the spherulites were directly measured under an optical microscope with crossed polarizers. For the measurement of G_H, PEO single crystals were grown from thin molten films with a thickness of about 100 nm, and examined with an electron microscope.

Five low molecular weight samples and one high molecular weight sample were investigated, and from Figure 4.7, G_R and G_H were found to agree extremely well with each other, showing no significant difference. Both growth rates extended over six orders of magnitudes, and they can be considered to belong to the higher temperature half of Figure 4.6, where the growth rate slows down as supercooling decreases. Along the curve of each low molecular weight, there was as least one sharp transition point. These points were believed to be transition temperatures $T(n)$, where the polymer chains in the crystal turned from n-times fold to $(n+1)$-times fold. The high molecular weight curve did not display such a transition point.

4.3 Optical microscopy experiments

With our purified products of PEO oligomers, we also did measurements on crystal growth rates under an optical microscope with crossed polarizers. With each sample, we watched crystallization, took a series of pictures at fixed time intervals, as shown in Figure 4.9, and measured the radius of a spherulite in each picture. A graph of crystal size as a function of crystallization time was then generated (Figure 4.10), and the growth rate was calculated from the slope of the graph. This process was repeated at different crystallization temperatures, and with fractions having different $\bar{N}$ values.

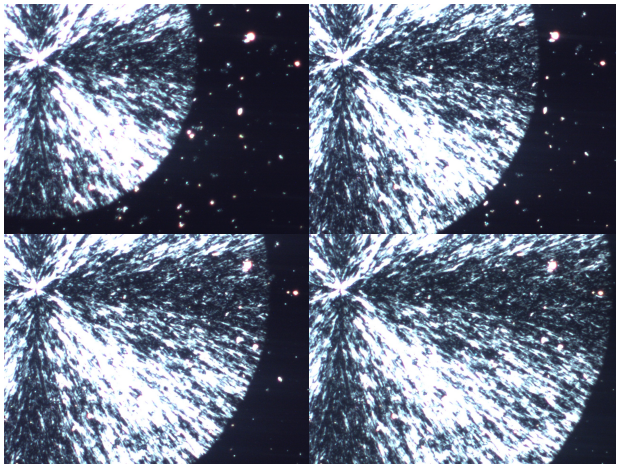

Figure 4.9: Four sequential images of fraction with $\bar{N} = 12.4$ at 260.65 K, under an optical microscope with crossed polarizers on.

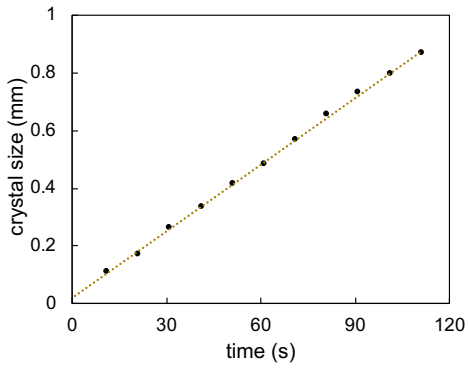

Figure 4.10: Crystal size as a function of crystallization time. $\bar{N} = 12.4$, $T = 260.65K$.

4.4 Crystal growth rate of purified products

We performed growth rate measurements with four of our fractions, and the results are shown in Figure 4.11.

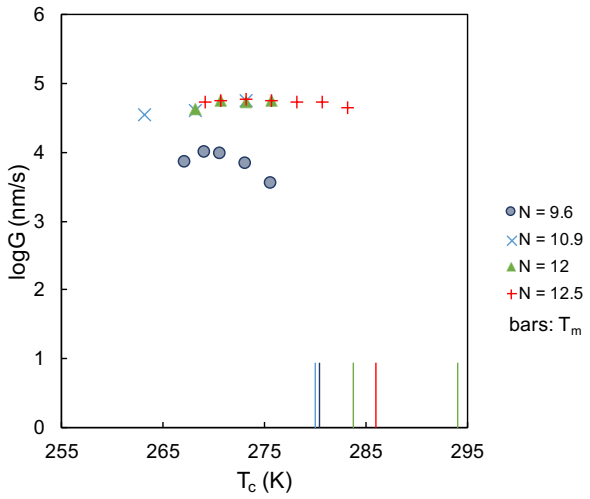

Figure 4.11: Crystal growth rate vs crystallization temperature, with four fractions having different chain lengths. Vertical bars are the melting temperatures of the fractions.

At low enough temperatures, the supercooling is large, and fast nucleation, fast crystal growth, and sufficiently bright contrast were obtained. However, at temperatures closer to T_m, the driving force became small due to small supercooling, which resulted in very difficult nucleation, and the contrast from the crystal was weak so that growth rate could not be measured successfully. Therefore, we have obtained data only for low crystallization temperatures and large growth rates. By looking at the graph itself, we could not find a clear trend, but comparison with Figure 4.7 showed good agreement between our data and the low temperature plateau regions in terms of scale in their study. In order to get the full picture of crystal growth of our samples, improvements in experiments are still required to allow us to measure crystallization under small supercoolings, and reach the rapidly decreasing regions as shown in Figure 4.8.

Chapter 5

Conclusion & discussion

To conclude, the three chapters in this thesis represent three major investigations conducted with oligomeric PEO: evaporative purification, chain-conformation, and crystal growth. We applied the evaporative purification technique to obtain highly monodisperse PEO oligomers. The purified products were examined by mass spectroscopy, in order to characterize the distribution of N's. With DSC and optical microscopy, we studied their crystallization and melting behaviours.

5.1 Evaporative purification of PEO

Through evaporative purification, the distribution of purified samples gets significantly narrowed down compared to that of the neat sample. Quantitatively the polydispersity is approximately six time better in the best case, according to the MALDI results. The evolution curves of different N values intuitively show that specific distribution of N's could be assigned to the evaporation time, which provides the possibility of commercializing this purification technique for low molecular weight polymers. In order to further reduce PDI, some practical improvements include: applying a larger mass of the neat sample; reducing collection intervals; carrying out multiple cycles of evaporation. As a matter of fact, PEO is not a perfect material in terms of this evaporation technique, as the vapour pressures of

different N values are not well separated. Comparing to those of polystyrene [16], the gaps between neighbouring vapour pressure curves of PEO are smaller, which results in more difficult separation through evaporation.

5.2 Chain conformation

The full extended length of the largest N we obtained ($N = 16$) is less than 5 nm, while polymer crystal lamella is commonly on the order of 10 nm in thickness [84]. Although the N values we have obtained are still considered small, and normally not expected to be able to fold, the best model to describe our T_m data from DSC measurements is that the higher T_m's adopt the extended chain mode, and the lower T_m's adopt the once-folded chain mode. Furthermore, the fact that we are able to eliminate the lower T_m and generate only the higher T_m through thermal treatment proves that we could tune the chain-folding mode from once-folded chains to extended chains, which is a direct validation of our model. For common commercial PEO oligomer samples, PDI is high, and the distribution over different chain lengths is broad, which potentially makes it difficult for all of them to make a single fold and form an ordered conformation in the lamella. However, when chain lengths are all similar, it is possible that the entropy of a once-folded lamella surface is lower, which makes this conformation more likely to exist. The measurement of crystallinity was limited by the instrumentation, and thus a larger scale of evaporation could also benefit crystallinity measurement.

5.3 Crystal growth

Processes, kinetics, and crystal structures in polymer crystal growth were reviewed in Chapter 4. Macrostructures named spherulites are formed in polymer crystal growth, and the measurements of PEO crystal growth rates were conducted based on the measurements of spherulite size under an optical microscope. The fact that nucleation rate is much slower than crystal growth rate enables us to conveniently carry out the growth rate measurement

independently. Due to the weak contrast at temperatures near T_m's, we have only obtained data for PEO crystallization under large supercoolings, which agree well with the data from low temperature regions in the literature. In future work, regions nearer melting temperatures should be examined. In addition, X-ray experiments would also be an ideal way to look further into the crystal lamellae.

References

[1] M. Rubinstein and R. H. Colby, *Polymer physics*. Oxford University Press, 2003.

[2] V. K. Thakur and M. K. Thakur, *Handbook of Sustainable Polymers: Processing and Applications*. CRC Press, 2016, illus. ed., 2016.

[3] C. E. Carraher, *Seymour/Carraher's polymer chemistry.* Taylor & Francis, 6, revised ed., 2003.

[4] R. J. Young, *Introduction to polymers, third edition.* CRC Press, 2017.

[5] N. A. Dotson, R. Galvan, R. L. Laurence, and M. Tirrell, *Polymerization Process Modeling*. John Wiley & Sons, illus. ed., 1996.

[6] J. Brady, T. Dürig, P. Lee, and J.-X. Li, "Polymer Properties and Characterization," *Dev. Solid Oral Dos. Forms*, pp. 181–223, 2017.

[7] C. P. Buckley and A. J. Kovacs, "Melting behaviour of low molecular weight poly (ethylene-oxide) fractions," in *Polym. Aspekte*, pp. 44–52, 1975.

[8] Z. Xue, D. He, and X. Xie, "Poly(ethylene oxide)-based electrolytes for lithium-ion batteries," *J. Mater. Chem. A*, vol. 3, no. 38, pp. 19218–19253, 2015.

[9] F. Croce, G. B. Appetecchi, L. Persi, and B. Scrosati, "Nanocomposite polymer electrolytes for lithium batteries," *Nature*, vol. 394, no. 6692, pp. 456–458, 1998.

[10] T. G. Fox and P. J. Flory, "Second-Order Transition Temperatures and Related Properties of Polystyrene. I. Influence of Molecular Weight," *J. Appl. Phys.*, vol. 21, no. 6, pp. 581–591, 1950.

[11] Y. Chai, *Surface Dynamics, Glass Transition, and Crystallization of Atactic Polystyrene*. PhD thesis, University of Waterloo, 2016.

[12] S. J. Organ, A. Keller, and G. Ungar, "Growth, Nucleation and Thickening Rate Minima in Long Linear Alkanes," in *Cryst. Polym.*, pp. 81–86, Dordrecht: Springer Netherlands, 1993.

[13] R. G. Alamo, "The Crystallization Behavior of Long Chain N-Alkanes and Low Molecular Weight Polyethylenes," in *Cryst. Polym.*, pp. 73–79, Dordrecht: Springer Netherlands, 1993.

[14] M. Anwar, F. Turci, and T. Schilling, "Molecular simulation of crystal nucleation in-octane melts," *Cit. J. Chem. Phys.*, vol. 139, p. 214904, 2013.

[15] T. Yamamoto, "Molecular dynamics of crystallization in n-alkane mixtures; texture, compatibility, and diffusion in crystals," *Polymer (Guildf).*, vol. 99, pp. 721–733, 2016.

[16] S. Zhu, Y. Chai, and J. A. Forrest, "Evaporative purification to produce highly monodisperse polymers: Application to polystyrene for n = 3 – 13 and quantification of T g from oligomer to polymer," *Phys. Rev. Mater.*, vol. 1, no. 2, p. 025605, 2017.

[17] U. K. Krieger, F. Siegrist, C. Marcolli, E. U. Emanuelsson, F. M. Gøbel, M. Bilde, A. Marsh, J. P. Reid, A. J. Huisman, I. Riipinen, N. Hyttinen, N. Myllys, T. Kurtén, T. Bannan, C. J. Percival, and D. Topping, "A reference data set for validating vapor pressure measurement techniques: homologous series of polyethylene glycols," *Atmos. Meas. Tech.*, vol. 11, pp. 49–63, 2018.

[18] I. C. Sanchez and R. H. Lacombe, "An elementary molecular theory of classical fluids. Pure fluids," *J. Phys. Chem.*, vol. 80, no. 21, pp. 2352–2362, 1976.

[19] P. A. Rodgers, "Pressure Volume Temperature Relationships for Polymeric Liquids: a Review of Equation of State and their Characteristic Parameters for 56 Polymers," *J. Appl. Polym. Sci.*, vol. 48, pp. 1061–1080, 1993.

[20] A. Choukourov, A. Grinevich, O. Polonskyi, J. Hanus, J. Kousal, D. Slavinska, and H. Biederman, "Vacuum Thermal Degradation of Poly(ethylene oxide)," *J. Phys. Chem. B*, vol. 113, pp. 2984–2989, 2009.

[21] G. R. Strobl, *The physics of polymers : concepts for understanding their structures and behavior*. Springer, 2007.

[22] K. Herrmann, O. Gerngross, and W. Abitz, "Zur Rontgenographischen Strukturforschung des Gelatinemicells.," *Z. Phys. Chem.*, vol. B10, pp. 371–394, 1930.

[23] P. J. Flory, *Principles of polymer chemistry*. Cornell University Press, 1953.

[24] P. J. Flory, "On the Morphology of the Crystalline State in Polymers," *J. Am. Chem. Soc.*, vol. 84, no. 15, pp. 2857–2867, 1962.

[25] P. Geil, "Polymer single crystals (Polymer reviews, Vol. 5), P. H. Geil, Interscience, New York, 1963," *J. Polym. Sci. Part A Gen. Pap.*, vol. 2, no. 4, pp. 2015–2016, 1964.

[26] H. G. Zachmann, "Der Einfluß der Konfigurationsentropie auf das Kristallisations- und Schmelzverhalten von hochpolymeren Stoffen," *Kolloid-Zeitschrift Zeitschrift für Polym.*, vol. 216-217, no. 1, pp. 180–191, 1967.

[27] H. G. Zachmann, "Statistische Thermodynamik des Kristallisierens und Schmelzens von hochpolymeren Stoffen," *Kolloid-Zeitschrift und Zeitschrift für Polym.*, vol. 231, no. 1-2, pp. 504–534, 1969.

[28] K. H. Storks, "An Electron Diffraction Examination of Some Linear High Polymers," *J. Am. Chem. Soc.*, vol. 60, no. 8, pp. 1753–1761, 1938.

[29] R. Jaccodine, "Observations of Spiral Growth Steps in Ethylene Polymer," *Nature*, vol. 176, no. 4476, pp. 305–306, 1955.

[30] P. H. Till, "The growth of single crystals of linear polyethylene," *J. Polym. Sci.*, vol. 24, no. 106, pp. 301–306, 1957.

[31] A. Keller, "A note on single crystals in polymers: Evidence for a folded chain configuration," *Philos. Mag.*, vol. 2, no. 21, pp. 1171–1175, 1957.

[32] A. J. Kovacs, C. Straupe, and A. Gonthier, "Isothermal growth, thickening, and melting of polyethylene oxide) single crystals in the bulk," *J. Polym. Sci. Polym. Symp.*, vol. 50, no. 1, pp. 283–325, 1975.

[33] D. Y. Yoon and P. J. Flory, "Molecular morphology in semicrystalline polymers," *Faraday Discuss. Chem. Soc.*, vol. 68, no. 0, p. 288, 1979.

[34] A. Keller, "Crystalline polymers; an introduction," *Faraday Discuss. Chem. Soc.*, vol. 68, no. 0, p. 145, 1979.

[35] W. Hu, *Polymer Physics: A Molecular Approach*. Springer, 2013.

[36] M. Zhang, B.-H. Guo, and J. Xu, "A Review on Polymer Crystallization Theories," *Crystals*, vol. 7, no. 1, p. 4, 2016.

[37] K. Yamada, M. Hikosaka, A. Toda, S. Yamazaki, and K. Tagashira, "Equilibrium Melting Temperature of Isotactic Polypropylene with High Tacticity: 1. Determination by Differential Scanning Calorimetry," *Macromolecules*, vol. 36, no. 13, pp. 4790–4801, 2003.

[38] J. P. Arlif, P. A. Spegt, and A. E. Skoulios, "Etude de la cristallisation des polymères I. Structure lamellaire de polyoxyéthylènes de faible masse moléculaire," *Die Makromol. Chemie*, vol. 99, no. 1, pp. 160–174, 1966.

[39] T. Yoshihara, H. Tadokoro, and S. Murahashi, "Normal vibrations of the polymer molecules of helical conformation. IV. Polyethylene oxide and polyethylene-d4oxide," *J. Chem. Phys.*, vol. 41, no. 9, pp. 2902–2911, 1964.

[40] Y. Takahashi and H. Tadokoro, "Structural Studies of Polyethers, (–(CH2)m–O–)n. X. Crystal Structure of Poly(ethylene oxide)," *Macromolecules*, vol. 6, no. 5, pp. 672–675, 1973.

[41] K. Okuyama, "Revisiting the Molecular Structure of Collagen," *Connect. Tissue Res.*, vol. 49, no. 5, pp. 299–310, 2008.

[42] A. J. Kovacs, C. Straupe, and A. Gonthier, "Isothermal growth, thickening, and melting of polyethylene oxide) single crystals in the bulk. II," *J. Polym. Sci. Polym. Symp.*, vol. 59, no. 1, pp. 31–54, 1977.

[43] C. P. Buckley and A. J. Kovacs, "Melting behaviour of low molecular weight poly (ethylene-oxide) fractions," *Colloid Polym. Sci.*, vol. 254, no. 8, pp. 695–715, 1976.

[44] D. Pfefferkorn, S. O. Kyerematen, K. Busse, H. W. Kammer, T. Thurn-Albrecht, and J. Kressler, "Crystallization and melting of poly(ethylene oxide) in blends and diblock copolymers with poly(methyl acrylate)," *Macromolecules*, vol. 44, no. 8, pp. 2953–2963, 2011.

[45] S. G. Yeates, H. H. Teo, R. H. Mobbs, and C. Booth, "Ethylene glycol oligomers," *Makromol. Chemie*, vol. 185, no. 8, pp. 1559–1563, 1984.

[46] V. Percec, C. Pugh, O. Nuyken, and S. D. Pask, "Macromonomers, Oligomers and Telechelic Polymers," in *Compr. Polym. Sci. Suppl.*, pp. 281–357, Elsevier, 1989.

[47] G. Jaeger, "The ehrenfest classification of phase transitions: Introduction and evolution," *Arch. Hist. Exact Sci.*, vol. 53, no. 1, pp. 51–81, 1998.

[48] International Organization for Standardization, *Plastics – Differential scanning calorimetry – Part 2: Determination of glass transition temperature and glass transition step height (ISO Standard No. 11357-2)*. 2013.

[49] J. H. Gibbs and E. A. DiMarzio, "Nature of the Glass Transition and the Glassy State," *J. Chem. Phys.*, vol. 28, no. 3, pp. 373–383, 1958.

[50] L. M. C. Janssen, "Mode-Coupling Theory of the Glass Transition: A Primer," *Front. Phys.*, vol. 6, p. 97, 2018.

[51] W. Götze, *Complex Dynamics of Glass-Forming Liquids: A Mode-Coupling Theory*. Oxford Scholarship Online, 2009.

[52] R. Wong, M. Ashton, and K. Dodou, "Effect of Crosslinking Agent Concentration on the Properties of Unmedicated Hydrogels," *Pharmaceutics*, vol. 7, no. 3, pp. 305–319, 2015.

[53] K. Pielichowski and K. Flejtuch, "Differential scanning calorimetry studies on poly(ethylene glycol) with different molecular weights for thermal energy storage materials," *Polym. Adv. Technol.*, vol. 13, no. 10-12, pp. 690–696, 2002.

[54] B. C. Okerberg, C. L. Soles, J. F. Douglas, H. W. Ro, A. Karim, and D. R. Hines, "Crystallization of Poly(ethylene oxide) Patterned by Nanoimprint Lithography," *Macromolecules*, vol. 40, pp. 2968–2970, 2007.

[55] J. Herzberger, K. Niederer, H. Pohlit, J. Seiwert, M. Worm, F. R. Wurm, and H. Frey, "Polymerization of Ethylene Oxide, Propylene Oxide, and Other Alkylene Oxides: Synthesis, Novel Polymer Architectures, and Bioconjugation," *Chem. Rev.*, vol. 116, pp. 2170–2243, 2015.

[56] M. J. Richardson, "Thermodynamic behaviour of polyethylene single crystals," *Trans. Faraday Soc.*, vol. 61, p. 1876, 1965.

[57] A. Keller, "A note on single crystals in polymers: Evidence for a folded chain configuration," *Philos. Mag.*, vol. 2, no. 21, pp. 1171–1175, 1957.

[58] G. Ungar and A. Keller, "Time-resolved synchrotron X-ray study of chain-folded crystallization of long paraffins," *Polymer (Guildf).*, vol. 27, no. 12, pp. 1835–1844, 1986.

[59] X. Zeng and G. Ungar, "Lamellar structure of non-integer folded and extended long-chain n-alkanes by small-angle X-ray diffraction," *Polymer (Guildf).*, vol. 39, no. 19, pp. 4523–4533, 1998.

[60] A. Marshall, R. C. Domszv, H. H. Teo, R. H. Mobbs, and C. Booth, "Crystallinity of Ethylene Oxide Oligomers," *Eur. Polym. J.*, vol. 17, no. 893, 1981.

[61] F. A. Halden and W. D. Kingery, "Surface Tension at Elevated Temperatures. II. Effect of C, N, O and S on Liquid Iron Surface Tension and Interfacial Energy with Al2O3," *J. Phys. Chem.*, vol. 59, no. 6, pp. 557–559, 1955.

[62] S. Jung, T. Ishikawa, S. Sekizuka, and H. Nakae, "Effects of sulfur on interfacial energy between Fe-C melt and graphite," *J. Mater. Sci.*, vol. 40, no. 9-10, pp. 2227–2231, 2005.

[63] R. Majumdar, K. S. Alexander, and A. T. Riga, "Physical characterization of polyethylene glycols by thermal analytical technique and the effect of humidity and molecular weight," *Pharmazie*, vol. 65, pp. 343–347, 2010.

[64] C. Vasile, *Handbook of polyolefins.* Taylor & Francis, 2 ed., 2000.

[65] F. Khoury and E. Passaglia, "The Morphology of Crystalline Synthetic Polymers," in *Treatise Solid State Chem.*, pp. 335–496, Springer US, 1976.

[66] L. Sawyer, D. T. Grubb, and G. F. Meyers, *Polymer Microscopy.* Springer Science & Business Media, 2008, 3 ed., 2008.

[67] D. I. Bower, *An Introduction to Polymer Physics.* Cambridge University Press, 2002, illus. ed., 2002.

[68] J. D. Hoffman and R. L. Miller, "Kinetic of crystallization from the melt and chain folding in polyethylene fractions revisited: theory and experiment," *Polymer (Guildf).*, vol. 38, no. 13, pp. 3151–3212, 1997.

[69] D. Turnbull and J. C. Fisher, "Rate of Nucleation in Condensed Systems," *J. Chem. Phys.*, vol. 17, no. 1, pp. 71–73, 1949.

[70] M. V. Massa and K. Dalnoki-Veress, "Homogeneous Crystallization of Poly(Ethylene Oxide) Confined to Droplets: The Dependence of the Crystal Nucleation Rate on Length Scale and Temperature," *Phys. Rev. Lett.*, vol. 92, no. 25, p. 255509, 2004.

[71] A. Röttele, T. Thurn-Albrecht, J.-U. S. And, and G. Reiter, "Thermodynamics of Formation, Reorganization, and Melting of Confined Nanometer-Sized Polymer Crystals," *Macromolecules*, vol. 36, pp. 1257–1260, 2003.

[72] A. Fick, "Ueber Diffusion," *Ann. der Phys. und Chemie*, vol. 170, no. 1, pp. 59–86, 1855.

[73] A. Fick, "On liquid diffusion," *J. Memb. Sci.*, vol. 100, pp. 33–38, 1995.

[74] H. Ouyang, C.-C. Chen, S. Lee, and H. Yang, "Acetone transport in poly(ethylene terephthalate) and related phenomena," *J. Polym. Sci. Part B Polym. Phys.*, vol. 36, no. 1, pp. 163–169, 1998.

[75] H. Ouyang and S.-H. Shore, "The mass transport in poly(ethylene terephthalate) and related induced-crystallization," *Polymer (Guildf).*, vol. 40, no. 19, pp. 5401–5406, 1999.

[76] H. Ouyang, W.-H. Lee, W. Ouyang, S.-T. Shiue, and T.-M. Wu, "Solvent-Induced Crystallization in Poly(ethylene terephthalate) during Mass Transport: Mechanism and Boundary Condition," *Macromolecules*, vol. 37, pp. 7719–7723, 2004.

[77] N. Naga, Y. Yoshida, K. Noguchi, and S. Murase, "Crystallization of Amorphous Poly(Lactic Acid) Induced by Vapor of Acetone to Form High Crystallinity and Transparency Specimen," *Open J. Polym. Chem.*, vol. 03, no. 02, pp. 29–33, 2013.

[78] J. I. Lauritzen and J. D. Hoffman, "Theory of Formation of Polymer Crystals with Folded Chains in Dilute Solution," *J. Res. Natl. Bur. Stand. Phys. Chem.*, vol. 64, no. 1, 1960.

[79] J. D. Hoffman and J. I. j. Lauritzen, "Crystallization of Bulk Polymers With Chain Folding: Theory of Growth of Lamellar Spherulites," *J. Res. Natl. Bur. Stand. Phys. Chem.*, vol. 65A, no. 4, 1961.

[80] J. I. Lauritzen and J. D. Hoffman, "Extension of theory of growth of chain-folded polymer crystals to large undercoolings," *J. Appl. Phys.*, vol. 44, no. 10, pp. 4340–4352, 1973.

[81] S. Z. Cheng and B. Lotz, "Enthalpic and entropic origins of nucleation barriers during polymer crystallization: the Hoffman–Lauritzen theory and beyond," *Polymer (Guildf).*, vol. 46, no. 20, pp. 8662–8681, 2005.

[82] J. D. Hoffman, "Regime III crystallization in melt-crystallized polymers: The variable cluster model of chain folding," *Polymer (Guildf).*, vol. 24, no. 1, pp. 3–26, 1983.

[83] G. S. Ross and L. J. Frolen, "10. Nucleation and Crystallization," *Methods Exp. Phys.*, vol. 16, pp. 339–397, 1980.

[84] R. C. Savage, N. Mullin, and J. K. Hobbs, "Molecular Conformation at the Crystal-Amorphous Interface in Polyethylene," *Macromolecules*, vol. 48, no. 17, pp. 6160–6165, 2015.